Annihilation effects in $B \to \pi\pi$ from QCD light-cone sum rules

A. Khodjamirian,[1] Th. Mannel,[1] M. Melcher,[1] and B. Melić[2]

[1]*Theoretische Physik 1, Fachbereich Physik, Universität Siegen, D-57068 Siegen, Germany*
[2]*Theoretical Physics Division, Rudjer Bošković Institute, HR-10002 Zagreb, Croatia*
(Received 28 September 2005; published 16 November 2005)

Using the method of QCD light-cone sum rules, we calculate the $B \to \pi\pi$ hadronic matrix elements with annihilation topology. We obtain a finite result, including the related strong phase. Numerically, the annihilation effects in $B \to \pi\pi$ turn out to be small with respect to the factorizable emission mechanism. Our predictions, together with the earlier sum rule estimates of emission and penguin contributions, are used for the phenomenological analysis of $B \to \pi\pi$ channels. We predict a $\Delta I = 1/2$ transition amplitude which significantly differs from this amplitude extracted from the current data.

I. INTRODUCTION

Charmless B decays play an increasing role as a possible window to physics beyond standard model (for a review see. e.g., [1]). In particular, the decays of the type $B \to \pi\pi$ and $B \to K\pi, K\bar{K}$ are actively investigated using various approaches [2–12].

One promising method to evaluate charmless nonleptionic B decays is QCD factorization (QCDF) [2,3], which to leading order in $1/m_b$ and $\alpha_s(m_b)$ yields the well-known formulae of naive factorization. However, even when QCD corrections and estimates for the penguin contributions are included, QCDF is only marginally consistent with the data for $B \to \pi\pi$. As a more general analysis of data shows, one indeed needs additional contributions to the decay amplitudes which correspond to the $\Delta I = 1/2$ piece of the Hamiltonian. Comparing with different topologies of the decay diagrams, this means an enhancement of either the penguin or annihilation contributions. Especially interesting is the weak annihilation (or weak exchange) of the b quark and the light antiquark in the B meson. In QCDF, formally suppressed as $1/m_b$, the annihilation contribution is divergent. Fits of QCDF to data [4], with the annihilation part replaced by finite parameters, yield large effects. Importantly, the fits themselves cannot clearly distinguish between the annihilation and penguin mechanisms. In order to assess the relative importance of the annihilation contribution, one needs a different approach in QCD which allows to calculate $B \to \pi\pi$ hadronic matrix elements with various topologies.

In the present paper we will employ the technique suggested in [13]. It is based on light-cone sum rules (LCSR) [14], the method which adapts the general idea of QCD sum rules [15] for the amplitudes of exclusive hadronic processes. One well-known application of LCSR is the calculation of the $B \to \pi$ form factor [16]. In the sum rule approach, as opposed to QCDF or to the perturbative hard-scattering QCD approach (PQCD) [6], one does not directly represent the hadronic matrix element in terms of quark-gluon diagrams. The QCD calculation takes place for the correlation function, a more general object, where

the separation of short and long-distance parts into hard-scattering amplitudes and pion distribution amplitudes (DA's), respectively, is possible "by construction," that is, due to an appropriate choice of kinematical variables. Both hard and soft-gluon effects are systematically included in this calculation, contributing to different terms of the light-cone operator-product expansion (OPE). The hard-gluon exchanges enter the hard-scattering amplitudes, whereas the soft-gluon effects are represented by quark-antiquark-gluon DA's of the pion. The hadronic matrix element appears as a part of the hadronic dispersion relation for the correlation function. Matching this relation to the result of the QCD calculation, one employs quark-hadron duality to separate the ground-state $B \to \pi\pi$ amplitude from the background of excited hadrons. The advantage of this technique, as will be explained in more details further, is a possibility to associate different decay topologies in the hadronic matrix element with the corresponding diagrams in the OPE, hence the relative contributions of various operators and topologies to the decay amplitude can be estimated. Importantly, the calculation of $B \to \pi\pi$ amplitudes takes place in full QCD at finite m_b and one uses the same input as in the sum rule for the $B \to \pi$ form factor. The latter provides also the factorizable part of the $B \to \pi\pi$ amplitude.

Penguin-topology contributions to $B \to \pi\pi$ have been estimated using LCSR already in previous papers [17,18], while annihilation topologies are notoriously difficult to calculate. This is due to the fact that the factorizable contribution of the current-current operators $O_{1,2}$ with annihilation topology vanishes. Hence, in a sum rule calculation, the leading nonfactorizable annihilation with one hard-gluon exchange already corresponds to a set of two-loop diagrams with several scales (b quark mass and external momenta).

In the present paper we employ a simplified method for the annihilation via hard gluons, that is, both final state pions are replaced by DA's and only the initial state B meson is interpolated by an appropriate current. Importantly, the propagators appearing in the resulting

Feynman diagrams carry sufficient virtuality to be treated perturbatively. Although this is a modification of the original idea presented in [13], it is a useful approach, since it yields a result free of infrared divergences. This result may be compared to what is obtained from QCDF, where an infrared regulator needs to be introduced, reducing basically the whole annihilation contribution to a nonperturbative parameter of order $1/m_b$. On the other hand, the annihilation with soft-gluon exchange which is not accessible in QCDF, is calculated here within the standard procedure [13] leading also to a finite answer. After adding the hard and soft-gluon contributions from LCSR, we obtain the main result: the finite matrix element of the operator O_1 with annihilation topology, including its phase. We predict this effect to be numerically small.

Furthermore, we investigate the annihilation contributions via quark-penguin operators. While $O_{3,4}$ have the same $V - A$ structure as $O_{1,2}$, so that the factorizable annihilation vanishes, the operators $O_{5,6}$ contribute through two different types of contractions. One of them has a $V + A$ content and also vanishes in the factorizable annihilation, whereas the other one, with a $S \pm P$ structure allows for a factorizable $B \to \pi\pi$ transition with annihilation topology. This contribution reduces to a separate nonperturbative object, the pion scalar form factor at timelike momentum transfer m_B^2. In QCDF and PQCD, the factorizable annihilation was taken into account only with a perturbative gluon exchange between the final state quarks, corresponding to the pion form factor in $O(\alpha_s)$. The method of LCSR allows to obtain the zeroth order in α_s, that is the "soft" (end-point) part of the scalar pion form factor. We calculate this part, with the same approach as for the e.m. (vector) pion form factor in [19,20]. The resulting hadronic matrix element is large, due to the chirally enhanced factor. Still this effect alone cannot produce a large $\Delta I = 1/2$ amplitude in $B \to \pi\pi$, because of the small Wilson coefficients.

Finally, we evaluate the $B \to \pi\pi$ decay amplitudes using LCSR predictions and including all calculated nonfactorizable effects with the emission, penguin, and annihilation topology. Since these effects are generally small, the discrepancy between the $B^0 \to \pi^+\pi^-$, $\pi^0\pi^0$ observables calculated in the factorization limit and the current experimental data remains. One may encounter a situation similar to $K \to \pi\pi$, with its long-standing problem of $\Delta I = 1/2$ rule.

The paper is organized as follows: In Section II we summarize the current status of phenomenology of $B \to \pi\pi$ amplitudes, starting from the isospin decomposition and naive factorization and comparing them with the data. In Section III we discuss nonfactorizable effects, representing the $B \to \pi\pi$ decay amplitudes in terms of hadronic matrix elements of effective operators with different topologies. In Section IV, we derive the LCSR for the hadronic matrix element of an effective operator with a given topology. In Sections V and VI we present our new results for

$B \to \pi\pi$ annihilation with perturbative (hard) and nonperturbative (soft) gluons, respectively.   In Section VII we obtain the sum rule for the pion scalar form factor which determines the specific factorizable annihilation contribution of the operators $O_{5,6}$. In Section VIII, we perform the numerical analysis and present the LCSR prediction for the annihilation contributions to $\bar{B}^0 \to \pi^+\pi^-$. Furthermore, we add all calculated contributions and present our numerical predictions for the branching ratios and direct CP asymmetries in all three $B \to \pi\pi$ channels. In Section IX we analyze our result in the limit $m_b \to \infty$ and comment on the annihilation mechanism in QCDF and PQCD. We conclude in Section X. The appendices contain some expressions used in the paper.

II. PHENOMENOLOGY OF $B \to \pi\pi$ AMPLITUDES

Throughout this paper we adopt isospin symmetry. We also neglect the effects of the electroweak penguin operators, so that the effective weak Hamiltonian for $B \to \pi\pi$ has the following expression:

$$H_{\text{eff}} = \frac{G_F}{\sqrt{2}}\{\lambda_u(c_1 O_1^u + c_2 O_2^u) + \lambda_c(c_1 O_1^c + c_2 O_2^c)$$

$$+ (\lambda_u + \lambda_c)[\sum_{i=3}^{6} c_i O_i + c_{8g} O_{8g}]\} + \text{H.c.} \qquad (1)$$

The CKM factors are defined as $\lambda_p = V_{pb}V_{pd}^*$ ($p = u, c, t$), and we use the CKM unitarity replacing $-\lambda_t$ by $\lambda_u + \lambda_c$. Hereafter we suppress for brevity the scale dependence in the Wilson coefficients c_i, which is supposed to be compensated by the scale dependence of the hadronic matrix elements of the effective operators O_i. The current-current operators entering Eq. (1) are

$$O_1^p = (\bar{d}\Gamma_\mu p)(\bar{p}\Gamma^\mu b) = \frac{1}{3} O_2^p + 2\tilde{O}_2^p,$$

$$O_2^p = (\bar{p}\Gamma_\mu p)(\bar{d}\Gamma^\mu b) = \frac{1}{3} O_1^p + 2\tilde{O}_1^p, \qquad (2)$$

where $p = u, c$, $\Gamma_\mu = \gamma_\mu(1 - \gamma_5)$, and

$$\tilde{O}_1^p = \left(\bar{d}\Gamma_\mu \frac{\lambda^a}{2} p\right)\left(\bar{p}\Gamma^\mu \frac{\lambda^a}{2} b\right),$$

$$\tilde{O}_2^p = \left(\bar{p}\Gamma_\mu \frac{\lambda^a}{2} p\right)\left(\bar{d}\Gamma^\mu \frac{\lambda^a}{2} b\right) \qquad (3)$$

with $\text{Tr}(\lambda_a\lambda_b) = 2\delta_{ab}$. The color Fierz transformation allows to use, instead of the combination $c_1 O_1^p + c_2 O_2^p$, either $(c_1 + c_2/3)O_1^p + 2c_2\tilde{O}_1^p$ or the opposite one with $1 \leftrightarrow 2$. In leading order the operators with color-neutral currents factorize and nonfactorizable contributions start from two-gluon exchanges, which we will neglect. The color-octet currents yield nonfactorizable effects starting at a one-gluon level. These effects will be systematically taken into account.

To complete the definition of H_{eff}, we specify the quark-penguin operators:

$$O_3 = \sum_f (\bar{f}\Gamma_\mu f)(\bar{d}\Gamma^\mu b) = \frac{1}{3}O_4 + 2\tilde{O}_4,$$

$$O_4 = \sum_f (\bar{d}\Gamma_\mu f)(\bar{f}\Gamma^\mu b) = \frac{1}{3}O_3 + 2\tilde{O}_3, \qquad (4)$$

$$O_5 = \sum_f (\bar{f}\gamma_\mu(1 + \gamma_5)f)(\bar{d}\Gamma^\mu b) = \frac{1}{3}O_6 + 2\tilde{O}_6,$$

$$O_6 = -2\sum_f (\bar{d}(1 + \gamma_5)f)(\bar{f}(1 - \gamma_5)b) = \frac{1}{3}O_5 + 2\tilde{O}_5,$$

where $f = u, d, s, c, b$ and we again use the color Fierz decompositions introducing the operators with color-octet currents $\tilde{O}_{3,4,5,6}$ obtained from $O_{3,4,5,6}$, respectively. Finally, the chromomagnetic quark-gluon penguin operator is:

$$O_{8g} = -\frac{g_s}{8\pi^2}m_b\bar{d}\sigma_{\mu\nu}(1 + \gamma_5)G^{\mu\nu}b. \qquad (5)$$

Turning to the phenomenology of $B \to \pi\pi$ we begin with quoting the results of the current measurements [21]:

$$BR(B^+ \to \pi^+\pi^0) = (5.5 \pm 0.6) \times 10^{-6},$$

$$BR(B^0 \to \pi^+\pi^-) = (5.0 \pm 0.4) \times 10^{-6}, \qquad (6)$$

$$BR(B^0 \to \pi^0\pi^0) = (1.45 \pm 0.29) \times 10^{-6},$$

where only the first branching ratio is compatible with the expectations of factorization.

The problem may be analyzed in terms of the usual isospin decomposition. The effective Hamiltonian of the standard model consists of two parts with $\Delta I = 1/2$ and $\Delta I = 3/2$, resulting in two reduced isospin amplitudes A_0 and A_2 in $B \to \pi\pi$, which correspond to the pions in the $I = 0$ and $I = 2$ final states, respectively. One obtains the following decomposition for the amplitudes[1]

$$A(B^- \to \pi^-\pi^0) = \langle\pi^-\pi^0|H_{\text{eff}}|B^-\rangle = \frac{3}{\sqrt{2}}A_2,$$

$$A(\bar{B}^0 \to \pi^+\pi^-) = \langle\pi^+\pi^-|H_{\text{eff}}|\bar{B}^0\rangle = A_2 + A_0, \qquad (7)$$

$$A(\bar{B}^0 \to \pi^0\pi^0) = \langle\pi^0\pi^0|H_{\text{eff}}|\bar{B}^0\rangle = 2A_2 - A_0,$$

from which the well-known isospin relation [22] is obtained:

$$A(\bar{B}^0 \to \pi^0\pi^0) = \sqrt{2}A(B^- \to \pi^-\pi^0) - A(\bar{B}^0 \to \pi^+\pi^-). \qquad (8)$$

---

[1]Throughout this paper we consider, for definiteness, B^- and $\bar{B}^0$ decay amplitudes, whereas all quoted branching ratios for B^+ and B^0 are, as usual, CP averaged.

In the above we use the same convention for the amplitudes, as in Refs. [2,3], including the statistical factor $1/2$ in the branching ratio for $\bar{B}^0 \to \pi^0\pi^0$.

From Eq. (7) one obtains the ratio of the moduli of A_0/A_2 in terms of the decay rates

$$\frac{|A_0|}{|A_2|} = \sqrt{3\left[\frac{BR(\bar{B}^0 \to \pi^0\pi^0) + BR(\bar{B}^0 \to \pi^+\pi^-)}{BR(B^- \to \pi^-\pi^0)}\right]\frac{\tau_{B^-}}{\tau_{B^0}} - 2}. \qquad (9)$$

Using Eq. (6) (neglecting CP asymmetries) and $\tau_{B^-}/\tau_{B^0} = 1.075 \pm 0.009$ [21], one gets

$$\frac{|A_0|}{|A_2|} = 1.33 \pm 0.31. \qquad (10)$$

Employing the tree-level emission graphs and retaining only the current-current operators (the *naive factorization* limit) we may obtain a first insight into the anatomy of these decays. In fact, this simplified way leads practically to the same conclusions as the full calculation in the framework of QCDF. First of all, the decay $B^- \to \pi^-\pi^0$ is well described in the factorization limit, where

$$\sqrt{2}A(B^- \to \pi^-\pi^0) = \lambda_u\frac{4}{3}(c_1(\mu) + c_2(\mu))\mathcal{A}_{\pi\pi} \qquad (11)$$

with the usual notations for the Wilson coefficients $c_{1,2}$ and the factorizable $B \to \pi\pi$ amplitude

$$\mathcal{A}_{\pi\pi} = i\frac{G_F}{\sqrt{2}}f_\pi f_{B\pi}^0(m_\pi^2)(m_B^2 - m_\pi^2). \qquad (12)$$

In the above, $f_\pi = 131$ MeV is the pion decay constant and $f_{B\pi}^0(q^2)$ is the scalar $B \to \pi$ form factor. Hereafter, we neglect m_π in the amplitudes, retaining it only in the ratio $\mu_\pi = m_\pi^2/(m_u + m_d)$.

In the factorization approximation, it is sufficient to use the leading-order (LO) values of the Wilson coefficients. We vary their renormalization scale within $m_b/2 < \mu < m_b$; for illustrative purpose we also put $\mu = M_W$. Using the LCSR prediction [16] for the $B \to \pi$ form factor:

$$f_{B\pi}^0(m_\pi^2) \simeq f_{B\pi}^0(0) = f_{B\pi}^+(0) = 0.26 \pm 0.05, \qquad (13)$$

which is explained below in Section VIII, and taking $|V_{ub}| = (4.22 \pm 0.11 \pm 0.24) \times 10^{-3}$ from Ref. [23] (adding the errors in quadrature) we obtain from Eq. (11)

$$BR(B^+ \to \pi^+ \pi^0)_{\text{fact}} = \begin{cases} (5.7^{+2.4}_{-2.0} \pm 0.7) \times 10^{-6}, & \mu = m_b/2 \quad (c_1 = 1.169, c_2 = -0.361) \\ (6.4^{+2.7}_{-2.3} \pm 0.8) \times 10^{-6}, & \mu = m_b \quad (c_1 = 1.108, c_2 = -0.249) \\ (8.7^{+3.7}_{-3.0} \pm 1.1) \times 10^{-6}, & \mu = M_W \quad (c_1 = 1, c_2 = 0), \end{cases} \tag{14}$$

where the errors reflect the uncertainties of the form factor and of $|V_{ub}|$, respectively. The scale dependence is mild, as expected.

Another way to check the validity of the factorization approximation for this channel (independent of $|V_{ub}|$ and the value of $f^+_{B\pi}(0)$) is provided by the ratio of the $B^+ \to \pi^+ \pi^0$ and $B^0 \to \pi^- l^+ \nu_l$ widths. In factorization approximation:

$$\frac{BR(B^+ \to \pi^+ \pi^0)}{BR(B^0 \to \pi^- l^+ \nu_l)}$$
$$= \frac{2\pi^2 |V_{ud}|^2 (c_1(\mu) + c_2(\mu))^2 f_\pi^2 m_B^3}{3 \int_0^{(m_B - m_\pi)^2} dq^2 (E_\pi^2 - m_\pi^2)^{3/2} |N_{B\pi}(q^2)|^2} \left(\frac{\tau_{B^+}}{\tau_{B_0}} \right), \tag{15}$$

where $E_\pi = (m_B^2 + m_\pi^2 - q^2)/(2m_B)$ and $N_{B\pi}(q^2) = f^+_{B\pi}(q^2)/f^+_{B\pi}(0)$ is the shape of the form factor. The recent measurement [24] of the $B \to \pi l \nu$ decay distribution, fitted to the parametrization [25], $N_{B\pi}(q^2) = [(1 - q^2/m_{B^*}^2)(1 - \alpha_{B\pi} q^2/m_{B^*}^2)]^{-1}$, yields $\alpha_{B\pi} = 0.61 \pm 0.09$. Using this value, and the average experimental number $BR(B^0 \to \pi^- l^+ \nu_l) = (1.36 \pm 0.11) \times 10^{-4}$ [21], we obtain at $\mu = m_b/2[m_b; M_W]$:

$$BR(B^+ \to \pi^+ \pi^0)_{\text{fact}} = (3.6 \pm 0.3 \pm 0.4) \times 10^{-6}$$
$$[(4.1 \pm 0.3 \pm 0.5) \times 10^{-6};$$
$$(5.6 \pm 0.5 \pm 0.6) \times 10^{-6}], \tag{16}$$

where the first error originates from the semileptonic branching ratio, and the second one from the slope parameter $\alpha_{B\pi}$. The result is again in the ballpark of the experimental interval (6). Hence we conclude that the amplitude A_2 may be estimated correctly by naive factorization.

Furthermore, using naive factorization, we may express the ratio A_0/A_2 in terms of the Wilson coefficients, since all hadronic matrix elements will drop out. Using Eq. (11) and the analogous relation

$$A(\bar{B}^0 \to \pi^+ \pi^-) = \lambda_u \left(c_1(\mu) + \frac{c_2(\mu)}{3} \right) \mathcal{A}_{\pi\pi}, \tag{17}$$

and comparing with the decomposition (7) we obtain

$$\frac{A_0}{A_2} = \frac{5}{4} \left(\frac{c_1(\mu) - c_2(\mu)/5}{c_1(\mu) + c_2(\mu)} \right) = \begin{cases} 1.92, & \mu = m_b/2 \\ 1.68, & \mu = m_b \\ 1.25, & \mu = M_W. \end{cases} \tag{18}$$

In fact, this expression depends quite strongly on the scale, showing that naive factorization for B^0 modes is compatible with the data only for a large scale of $O(m_W)$, which seems unrealistic.

A more distinct disagreement is revealed between the ratios of B^0 and B^+ partial widths calculated in the naive factorization at $\mu = m_b/2[m_b; M_W]$:

$$\frac{BR(B^0 \to \pi^+ \pi^-)}{BR(B^+ \to \pi^+ \pi^0)} = 1.77[1.49; 1.05],$$
$$\frac{BR(B^0 \to \pi^0 \pi^0)}{BR(B^+ \to \pi^+ \pi^0)} \simeq 10^{-3}[0.010; 0.058], \tag{19}$$

and the same ratios obtained from the experimental results (6). In fact, the calculated $B \to \pi^0 \pi^0$ width is too small even at $\mu = m_W$. We conclude that the naive factorization picture misses an important part of the amplitude A_0 which interferes destructively (constructively) with A_2 in $A(\bar{B}^0 \to \pi^+ \pi^-)$ ($A(\bar{B}^0 \to \pi^0 \pi^0)$). If there were large nonfactorizable gluon corrections to the emission topology, they would have influenced both A_0 and A_2, violating the above-mentioned agreement for the $B^- \to \pi^- \pi^0$ channel. Hence, the missing isospin zero amplitude should be searched for within the contributions of nonemission topologies for the current-current operators and/or in the contributions of the penguin operators, an opinion shared by many recent analyses of these decays.

III. BEYOND FACTORIZATION

In Fig. 1 we schematically represent different quark topologies contributing to the amplitude of $\bar{B}^0 \to \pi^+ \pi^-$, the channel of our interest. Under *topology* we understand the way to contract the valence quarks (antiquarks) of the initial B and final mesons with the antiquarks (quarks)
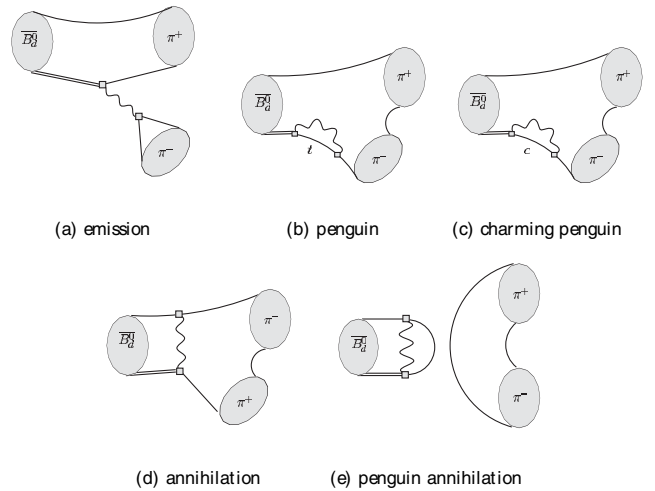

(a) emission   (b) penguin   (c) charming penguin

(d) annihilation   (e) penguin annihilation

FIG. 1. Different quark topologies in $\bar{B}^0 \to \pi^+ \pi^-$; double lines denote the b quark, wavy lines the W boson.

from the effective weak Hamiltonian. This concept is meaningful for all those methods where the valence quark structure of mesons is well defined, either via the meson distribution amplitudes (DA's) as, e.g. in QCDF, or via both DA's and interpolating currents, as in the correlation function for LCSR. Denoting the valence spectator antiquark in $\bar{B}$ by $\bar{q}_s$ and the quarks emitted in the b-quark decay by q_1, q_2, $\bar{q}_3$ we define *emission* as the part of the decay amplitude where all four quarks and antiquarks end up as the valence quarks of the final mesons [Fig. 1(a)]. Correspondingly *penguin* is the part where $\bar{q}_s$ and only one of q_1, q_2 belong to the final mesons [Figs. 1(b) and 1(c)]. The remaining two possibilities are *annihilation* [Fig. 1(d)] or *penguin annihilation* [Fig. 1(e)], where either $\bar{q}_3$ and the one of q_1, q_2 or none of the quarks are among the valence quarks of the final mesons, respectively.[2]

In the isospin symmetry limit it is sufficient to investigate in detail the $\bar{B}^0 \to \pi^+\pi^-$ amplitude. It has a single $I = 2$, $O(\lambda_u)$ part with emission topology, common with the $B^- \to \pi^-\pi^0$ amplitude, and in addition contains many different $I = 0$ contributions proportional to both λ_u and λ_c. The $\bar{B}^0 \to \pi^0\pi^0$ amplitude is then obtained by simply using the isospin relation (8).

The complete isospin decomposition of the $\bar{B}^0 \to \pi^+\pi^-$ amplitude following from Eq. (1) can be cast in the following form:

$$A(\bar{B}^0 \to \pi^+\pi^-) = \lambda_u(A_2^{(u,1,2)} + A_0^{(u,1,2)})$$
$$+ \lambda_c A_0^{(c,1,2)} + (\lambda_u + \lambda_c)A_0^{(\geq 3)}, \quad (20)$$

where the upper indices in $A_I^{(i)}$ indicate the contributing operators and the lower index the isospin. Correspondingly,

$$\sqrt{2}A(B^- \to \pi^-\pi^0) = \lambda_u(3A_2^{(u,1,2)}). \quad (21)$$

Each separate amplitude $A_I^{(i)}$ in Eqs. (20) and (21) contains a sum over hadronic matrix elements with different topologies (T): emission (E), penguin (P_q, P_c, P_b), annihilation (A), and penguin annihilation (P_qA, P_cA, P_bA), where $q = u, d, s$. According to Ref. [26], this subdivision can be systematically done in a scheme- and scale-independent way. It is clear, that the number of independent matrix elements of the type $\langle \pi^+\pi^-|O_i|\bar{B}^0\rangle_T$ is less than the number of operators because certain penguin operators have the same quark structure as the current-current operators. For the penguin topologies we will also neglect the differences between quark loops with $q = u, d, s$.

Let us first discuss the $I = 2$ part in Eqs. (20) and (21), which is relatively simple. Taking into account the non-

factorizable emission correction, where only $\tilde{O}_1^u$ contributes in the one-gluon approximation, we introduce the ratio:

$$r_E^{(\pi\pi)} = \frac{\langle \pi^+\pi^-|\tilde{O}_1^u|\bar{B}^0\rangle_E}{\langle \pi^+\pi^-|O_1^u|\bar{B}^0\rangle_E}. \quad (22)$$

Note that in the adopted approximation the matrix element standing in the denominator is factorizable: $G_F/\sqrt{2}\langle \pi^+\pi^-|O_1^u|\bar{B}^0\rangle_E = \mathcal{A}_{\pi\pi}$. We obtain:

$$A_2^{(u,1,2)} = \left[\frac{4}{9}(c_1 + c_2) + \frac{2}{3}(c_1 + c_2)r_E^{(\pi\pi)}\right]\mathcal{A}_{\pi\pi}. \quad (23)$$

Accordingly, the $I = 0$ part generated by the operators $O_{1,2}^u$ has the following decomposition:

$$A_0^{(u,1,2)} = \left[\frac{1}{9}(5c_1 - c_2) - \frac{2}{3}(c_1 - 2c_2)r_E^{(\pi\pi)}\right.$$
$$\left. + 2c_1(r_{P_u}^{(\pi\pi)} + r_A^{(\pi\pi)})\right]\mathcal{A}_{\pi\pi}, \quad (24)$$

where the relative contributions for penguin and annihilation topologies[3] similar to Eq. (22) are defined as follows:

$$r_{P_u}^{(\pi\pi)} = \frac{\langle \pi^+\pi^-|\tilde{O}_2^u|\bar{B}^0\rangle_{P_u}}{\langle \pi^+\pi^-|O_1^u|\bar{B}^0\rangle_E}, \quad r_A^{(\pi\pi)} = \frac{\langle \pi^+\pi^-|\tilde{O}_2^u|\bar{B}^0\rangle_A}{\langle \pi^+\pi^-|O_1^u|\bar{B}^0\rangle_E}. \quad (25)$$

Hereafter, we will use a more generic notation $r_{P_q}^{(\pi\pi)}$, $q = u, d, s$, so that $r_{P_u}^{(\pi\pi)} = r_{P_q}^{(\pi\pi)}$ in accordance with our approximation for the light-quark-penguin loops. Furthermore, the $O_{1,2}^c$ operators with c-quark contribute to Eq. (20) only in the penguin topology ("charming penguins"):

$$A_0^{(c,1,2)} = 2c_1 r_{P_c}^{(\pi\pi)}, \quad \text{where } r_{P_c}^{(\pi\pi)} = \frac{\langle \pi^+\pi^-|\tilde{O}_2^c|\bar{B}^0\rangle_{P_c}}{\langle \pi^+\pi^-|O_1^u|\bar{B}^0\rangle_E}. \quad (26)$$

The remaining piece of the decomposition (20) containing the hadronic matrix elements of quark-penguin operators with various topologies, normalized to the factorizable part, is more complicated:

---

[2]Note that drawing generic quarkline diagrams, one can always start from the emission topology and then, merging the quark-antiquark (spectator) lines in the final state, end up with an annihilation mechanism; according to our classification, this mechanism still belongs to annihilation.

[3]In this paper, we neglect the penguin-annihilation (PA) topologies. They can be simply added to the general decomposition by introducing the corresponding $r_{PA}^{(\pi\pi)}$ ratios, but from LCSR we expect them to be small; this mechanism is also neglected in QCDF.

$$A_0^{(\geq3)} = \left[c_4 + \frac{c_3}{3} + 2c_3(r_E^{(\pi\pi)} + r_{P_q}^{(\pi\pi)} + r_{P_b}^{(\pi\pi)} + r_A^{(\pi\pi)}) \right.$$

$$+ 2c_4(3\bar{r}_{P_q}^{(\pi\pi)} + \bar{r}_{P_c}^{(\pi\pi)} + \bar{r}_{P_b}^{(\pi\pi)} + 2r_A^{(\pi\pi)}) + \frac{2\mu_\pi}{m_b}$$

$$\times \left(c_6 + \frac{c_5}{3} \right) + 2c_5 r_E^{(\pi\pi,6)} + 2c_6(3\bar{r}_{P_q}^{(\pi\pi)} + \bar{r}_{P_c}^{(\pi\pi)}$$

$$+ \bar{r}_{P_b}^{(\pi\pi)} + 2r_A^{(\pi\pi,5)}) + \left(c_6 + \frac{c_5}{3} \right) R_A^{(\pi\pi,6)}$$

$$\left. + 2c_5 r_A^{(\pi\pi,6)} + c_{8g}^{\text{eff}} r_{8g}^{(\pi\pi)} \right] A\pi\pi. \tag{27}$$

Some of the $r_T^{(\pi\pi)}$-parameters entering the above equation have already been defined: we use the fact that certain quark-penguin and current-current operators coincide. The parameter $r_{P_b}^{(\pi\pi)}$ determines the relative contribution of the b-quark penguin topology. It is defined as in Eq. (26) with $c \to b$. Furthermore, the notation $\bar{r}_{P_{q,c,b}}^{(\pi\pi)}$ is introduced to distinguish the penguin contractions of the operators $O_{4,6}$ ($\tilde{O}_{3,5}$) from those of $O_{1,3}$ ($\tilde{O}_{2,4}$). In the NDR scheme used here, as in [2,3], the quark loop factors for the two contractions differ by a constant. The loop factor entering LCSR for $r_{P_{q,c,b}}^{(\pi\pi)}$ is given in Eq. (4) of [18]. To obtain the corresponding factor for $\bar{r}_{P_{q,c,b}}^{(\pi\pi)}$ one simply has to subtract $1/6$ from this expression. A few terms in Eq. (27) are generated by the effective operator O_6 with $(S + P) \otimes (S - P)$ structure. First, the factorizable emission contribution of the u-quark part of this operator, $O_6^u = -2(\bar{d}(1 + \gamma_5)u)(\bar{u}(1 - \gamma_5)b)$, acquires a "chirally enhanced" factor μ_π/m_b, whereas its nonfactorizable part is described by an additional parameter:

$$r_E^{(\pi\pi,6)} = \frac{\langle \pi^+\pi^- | \tilde{O}_6^u | \bar{B}^0 \rangle_E}{\langle \pi^+\pi^- | O_1^u | \bar{B}^0 \rangle_E}. \tag{28}$$

Second, there is a specific factorizable annihilation contribution due to the d-quark part of the same operator $O_6^d \equiv -2(\bar{d}(1 + \gamma_5)d)(\bar{d}(1 - \gamma_5)b)$ which is expressed in terms of the B meson decay constant $\langle 0 | \bar{d}\gamma_5 b | B \rangle = -im_B^2 f_B/m_b$ multiplied by the pion scalar form factor:

$$\langle \pi^+(p_1)\pi^-(p_2) | \bar{d}d | 0 \rangle = F_\pi^S((p_1 + p_2)^2), \tag{29}$$

corresponding to the transition of the scalar and isoscalar quark-antiquark current into a two-pion state with the invariant mass squared $(p_1 + p_2)^2 = m_B^2$. The parameter in Eq. (27) determining the annihilation via O_6^d is factorized as:

$$R_A^{(\pi\pi,6)} = \frac{\langle \pi^+\pi^- | O_6^d | \bar{B}^0 \rangle_A}{\langle \pi^+\pi^- | O_1^u | \bar{B}^0 \rangle_E} = -\frac{2f_B F_\pi^S(m_B^2)}{m_b f_\pi f_{B\pi}^+(0)}. \tag{30}$$

The nonfactorizable annihilation correction of the color-octet counterpart of this operator in Eq. (27) is parametrized as

$$r_A^{(\pi\pi,6)} = \frac{\langle \pi^+\pi^- | \tilde{O}_6^d | \bar{B}^0 \rangle_A}{\langle \pi^+\pi^- | O_1^u | \bar{B}^0 \rangle_E}. \tag{31}$$

In addition to this $S \pm P$ contractions, the nonfactorizable annihilation contribution from the $V + A$ contraction is defined in analogy to Eq. (31) with $(6 \to 5)$. Finally, the parameter in Eq. (27) describing the contribution of the gluonic penguin operator (with the penguin topology) is:

$$r_{8g}^{(\pi\pi)} = \frac{\langle \pi^+\pi^- | O_{8g} | \bar{B}^0 \rangle_{P_g}}{\langle \pi^+\pi^- | O_1^u | \bar{B}^0 \rangle_E}. \tag{32}$$

In the NDR scheme it should be multiplied by $c_{8g}^{\text{eff}} = c_{8g} - c_5$ (see [3]).

For convenience, in Appendix A we present the relations of the parameters $r_T^{(\pi\pi)}$ introduced above to the effective coefficients a_i and b_i used in QCDF [2,3] to encode the nonfactorizable effects in $B \to \pi\pi$. Equation (20) can also be converted into a typical decomposition in terms of "tree," "color-suppressed," and "penguin" amplitudes used in the CP analysis of charmless decays, where the separation to $\lambda_u = |\lambda_u|e^{-i\gamma}$ and λ_c parts is made explicit:

$$A(\bar{B}^0 \to \pi^+\pi^-) = e^{-i\gamma} T_{\pi\pi} + P_{\pi\pi},$$
$$\sqrt{2}A(B^- \to \pi^-\pi^0) = e^{-i\gamma}(T_{\pi\pi} + C_{\pi\pi}). \tag{33}$$

Comparing the above with Eq. (20) one reads off:

$$T_{\pi\pi} = |\lambda_u|(A_2^{(u,1,2)} + A_0^{(u,1,2)} + A_0^{(\geq3)}),$$
$$P_{\pi\pi} = \lambda_c(A_0^{(c,1,2)} + A_0^{(\geq3)}), \tag{34}$$
$$T_{\pi\pi} + C_{\pi\pi} = |\lambda_u|(3A_2^{(u,1,2)}).$$

To analyze the $B \to \pi\pi$ amplitudes in terms of separate isospin contributions, one needs the numerical values of the hadronic parameters entering Eqs. (23), (24), and (26), and (27). Some of them have already been estimated using LCSR. For the nonfactorizable emission entering through $r_E^{(\pi\pi)}$ we will partly use the QCDF result. The calculation of the unknown annihilation parameters $r_A^{(\pi\pi)}$ and $R_A^{(\pi\pi,6)}$ from LCSR is the main issue of this paper.

IV. DERIVATION OF LCSR

The method we apply is basically the one developed in [13], (see also [17,18]) with some important modifications which will be explained in this section. To demonstrate the derivation of LCSR for a generic hadronic matrix element $\langle \pi^+\pi^- | O | \bar{B}^0 \rangle_T$, let us choose for definiteness the combination of current-current operators $O = c_1 O_1^u + c_2 O_2^u$ at a fixed scale, considering it as a superposition of two local operators.

One starts from the correlation function

$$F_\alpha^{(O)}(p, q, k) = - \int d^4x\, e^{-i(p-q)x} \int d^4y\, e^{i(p-k)y}$$

$$\times \langle 0|T\{j_{\alpha5}^{(\pi)}(y)O^u(0)j_5^{(B)}(x)\}|\pi^-(q)\rangle, \quad (35)$$

where $j_{\alpha5}^{(\pi)} = \bar{u}\gamma_\alpha\gamma_5 d$ and $j_5^{(B)} = m_b \bar{b} i \gamma_5 d$ are the quark currents interpolating the pion and the B meson, respectively. The momentum k is artificial and will vanish in the final sum rule. It is introduced in order to have two independent kinematical variables in the B and $\pi\pi$ channels.

The correlator (35) can be decomposed into four different Lorentz structures,

$$F_\alpha^{(O)} = (p - k)_\alpha F^{(O)} + q_\alpha \tilde{F}_1^{(O)} + k_\alpha \tilde{F}_2^{(O)}$$

$$+ \epsilon_{\alpha\beta\gamma\rho} q^\beta p^\lambda k^\rho \tilde{F}_3^{(O)},$$

of which we use only the first. Concerning the kinematical variables, we put $q^2 = m_\pi^2 = 0$ and choose $p^2 = k^2 = 0$ for simplicity. The remaining invariants are $(p - k)^2$, $(p - q)^2$, and $P^2 \equiv (p - k - q)^2$. In the domain where all three variables are spacelike and large, all distances are close to the light-cone, $x^2 \sim y^2 \sim (x - y)^2 \sim 0$, and the correlation function can be calculated by perturbatively expanding the T product of operators. In this way, the correlation function is expressed in a usual form of hard-scattering amplitudes convoluted with pion DA's of growing twist.

For a given operator O in the correlation function (35), various contractions of the quark fields are possible, leading to diagrams with different topologies. Collecting the lowest-order contributions to OPE, we easily recognize diagrams with the emission (Fig. 2), penguin (Fig. 3), annihilation (Fig. 4), and penguin-annihilation (Fig. 5)
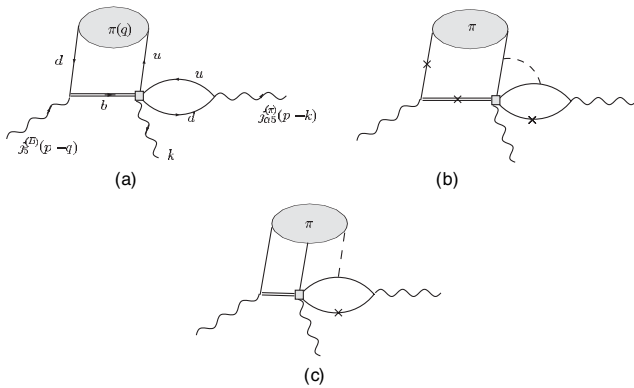
FIG. 2. Diagrams corresponding to the emission topology in the OPE of the correlation function (35): (a) factorizable; (b) with nonfactorizable hard gluon (six diagrams); (c) nonfactorizable soft gluon (two diagrams). The solid, double, dashed, wavy lines and the square denote the light quarks, b quark, gluon, external currents, and the weak vertex, respectively. The shaded ovals denote the pion DA's. The crosses indicate how gluon lines are attached in the other possible diagrams.
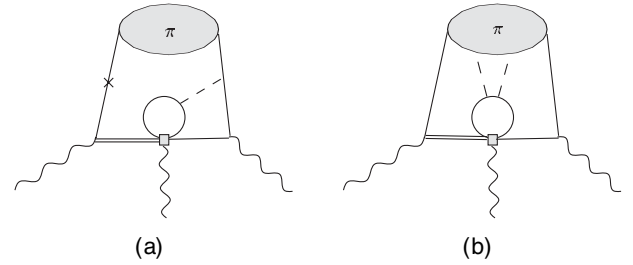
FIG. 3. Examples of diagrams corresponding to the penguin topology: with (a) hard gluon and (b) soft gluons.

topologies. The sum of all diagrams calculated at a definite order in OPE, will be matched to the dispersion relation where the ground-state contribution contains the hadronic matrix element $\langle \pi^+ \pi^- |O|\bar{B}^0\rangle$. If one retains only diagrams with a topology T in the OPE, the sum rule result (within adopted accuracy) can be interpreted as $\langle \pi^+ \pi^- |O|\bar{B}^0\rangle_T$.[4] This was actually done for the emission topology in [13] where the diagrams in Fig. 2 have been investigated. It was shown that retaining only the diagram of Fig. 2(a), without gluons connecting the light-quark loop and the heavy-light part, one reproduces the result of naive factorization. Importantly, the gluons which do not violate factorization in this diagram can be added arbitrarily. Altogether, one obtains the product of the LCSR for the $B \to \pi$ form factor and the two-point sum rule for the pion decay constant. The diagrams in Fig. 2(b) and 2(c) describe nonfactorizable corrections in the emission topology. The diagrams with soft gluons in Fig. 2(c) were calculated in [13]. Furthermore, penguin contractions for $O_{1,2}^p$ (some of diagrams are shown in Fig. 3) have also been studied in the framework of LCSR [18] allowing to calculate the parameters $r_{P_c}^{(\pi\pi)}$, $r_{P_b}^{(\pi\pi)}$, and $r_{P_q}^{(\pi\pi)}$. In addition, the LCSR for the gluonic penguin operator was derived in [17] yielding $r_{8g}^{(\pi\pi)}$. In the next two sections, we will present the calculation of the remaining diagrams with the annihilation topology (Fig. 4).

Having at hand the QCD calculation of a set of diagrams with topology T in terms of pion DA's and hard-scattering amplitudes, one can then express the correlation function in the form of a dispersion relation in the variable $s \equiv (p - k)^2$:

$$F_{QCD}^{(O,T)}((p - k)^2, (p - q)^2, P^2)$$

$$= \frac{1}{\pi} \int_0^\infty ds\, \frac{\mathrm{Im}_s F_{QCD}^{(O,T)}(s, (p - q)^2, P^2)}{s - (p - k)^2 - i\epsilon}. \quad (36)$$

---

[4]Since we are studying only the leading-order effects here and use a fixed scale, the scale and scheme dependence as well as the mixing effects between separate operators in H_{eff}, remain beyond our scope. To account for these effects one has to consider scale- and scheme-invariant combinations of matrix elements with different topologies as explained in [26].
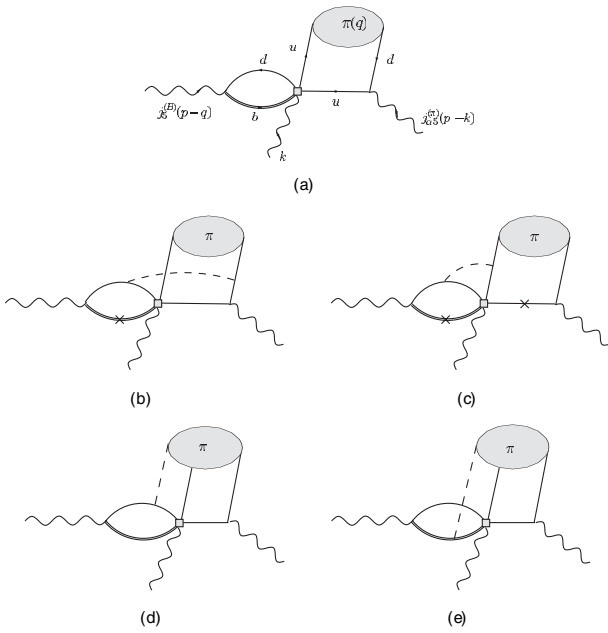
FIG. 4. Diagrams corresponding to the annihilation topology in the OPE of the correlation function (35): (a) factorizable; (b), (c) with hard gluon; (d), (e) with soft gluon.

On the other hand, one can insert a complete set of hadronic states in the π meson channel, and obtain

$$
\begin{aligned}
F^{(O,T)}&((p-k)^2, (p-q)^2, P^2) \\
&= \frac{if_\pi \Pi_{\pi\pi}^{(O,T)}((p-q)^2, P^2)}{-(p-k)^2} \\
&\quad + \int_{s_h^\pi}^\infty ds \frac{\rho_h^\pi(s, (p-q)^2, P^2)}{s - (p-k)^2},
\end{aligned}
\tag{37}
$$

where the one-pion ground-state contribution contains the pion decay constant and the matrix element

$$
\Pi_{\pi\pi}^{(O,T)}((p-q)^2, P^2) = i \int d^4x e^{-i(p-q)x}
$$
$$
\times \langle \pi^-(p-k)|T\{O(0)j_5^{(B)}(x)\}|\pi^-(q)\rangle_T, \tag{38}
$$

and ρ_h^π is the spectral density of heavier hadronic states in this channel. Replacing the integral over ρ_h^π with the standard duality approximation and equating (36) to (37), we obtain, after the usual Borel transformation:
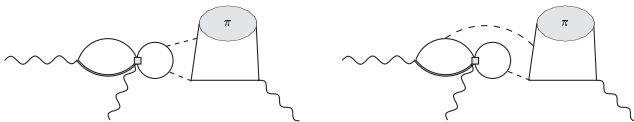

FIG. 5. Some of the lowest-order diagrams corresponding to the penguin-annihilation topology.
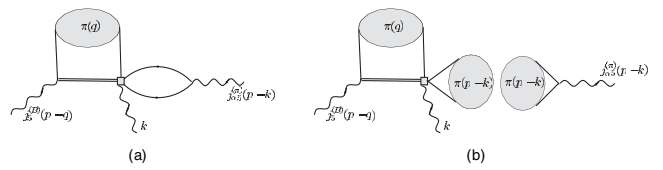

FIG. 6. The first step in the derivation of the sum rule for $B \to \pi\pi$ amplitude in the emission topology: (a) the initial correlation function (only diagrams with emission topology are included) is matched to (b) the hadronic dispersion relation in the pion channel where only the ground-state pion contribution is shown.

$$
\begin{aligned}
\Pi_{\pi\pi}^{(O,T)}((p-q)^2, P^2) = \frac{-i}{\pi f_\pi} \int_0^{s_0^\pi} ds \, e^{-s/M^2} \\
\times \text{Im}_s F_{\text{QCD}}^{(O,T)}(s + i\epsilon, (p-q)^2, P^2),
\end{aligned}
\tag{39}
$$

where s_0^π is the duality threshold in the pion channel. This first step in the derivation of LCSR is schematically shown in Fig. 6 where the diagrams with emission topology are chosen for definiteness.

Note that the hadronic matrix element (38) diagrammatically shown in Fig. 6(b) itself represents a correlator. At large negative $(p-q)^2$ and P^2 it can be factorized into a short-distance part (the b-quark propagator) and a long-distance part (the combination of two pion DA's). Adding hard-gluon exchanges does not seemingly spoil this factorization. In any case, the absence of infrared singularities has to be checked by a direct calculation. Hence, instead of using (39), we are free to use $\Pi_{\pi\pi}^{(O,T)}$ as a starting QCD object. That will be done below in the case of the annihilation topology with hard gluons, while employing the standard derivation of (39) for the soft-gluon part.

To continue, following [13] we consider $\Pi_{\pi\pi}^{(O,T)}((p-q)^2, P^2)$, as an analytical function of the variable P^2, the invariant mass of the $\pi\pi$ pair. Starting from our calculation for negative P^2, we have to reach the physical timelike point $P^2 = m_B^2$ by analytical continuation (see Fig. 7). As
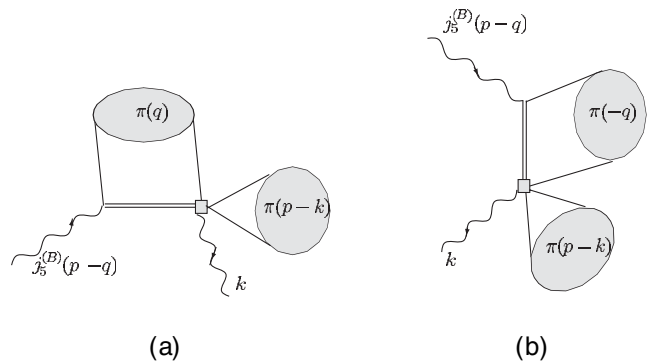

FIG. 7. The second step in the derivation of the sum rule: (a) the two-pion matrix element calculated in the spacelike region is analytically continued to (b) the same matrix element in the timelike region.
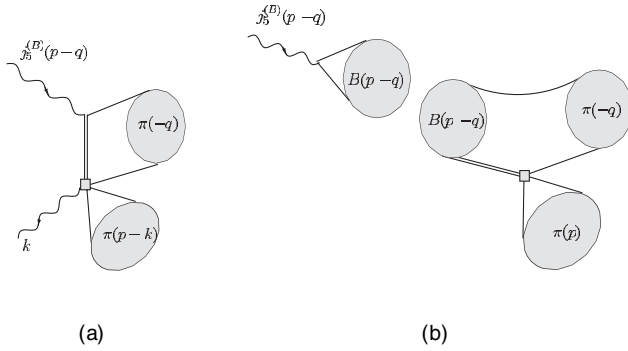
(a)   (b)

FIG. 8.   The third step in the derivation of the sum rule: (a) the two-pion matrix element $\prod_{\pi\pi}^{(O,E)}$ after analytic continuation to $(p-q-k)^2 = m_B^2$ is matched to (b) the hadronic dispersion relation in the B-meson channel; the ground-state B-meson contribution is proportional to the $B \to \pi\pi$ matrix element in emission topology.

already explained in [13], we use the fact that $m_B^2 \gg m_\pi^2, s_0^\pi$, i.e., the two-pion system in the B decay is in the timelike asymptotic region, far from the light-quark resonances. Note that at fixed $(p-q)^2$, the matrix element $\Pi_{\pi\pi}^{(O,T)}$ can always be represented in a form of a hadronic dispersion relation in the variable P^2:

$$\Pi_{\pi\pi}^{(O,T)}((p-q)^2, P^2) = \frac{1}{\pi} \int_0^\infty dt \frac{\text{Im}_t \Pi_{\pi\pi}^{(O,T)}((p-q)^2, t)}{t - P^2 - i\epsilon}. \tag{40}$$

This dispersion relation is only needed for illustrative purpose because it allows to unambiguously determine the point of analytical continuation we need as $P^2 = m_B^2 + i\epsilon$. Finally, it is convenient to represent the QCD calculation result $\Pi_{\pi\pi}^{(O,T)}((p-q)^2, m_B^2)$ in the form of the dispersion relation in the variable $(p-q)^2$,

$$\Pi_{\pi\pi}^{(O,T)}((p-q)^2, m_B^2 + i\epsilon) = \frac{1}{\pi} \int_{m_b^2}^\infty ds' \frac{\text{Im}_{s'} \Pi_{\pi\pi}^{(O,T)}(s', m_B^2)}{s' - (p-q)^2 - i\epsilon}, \tag{41}$$

and equate this to the hadronic representation in the B-meson channel (see Fig. 8),

$$\Pi_{\pi\pi}^{(O,T)}((p-q)^2, m_B^2 + i\epsilon)$$
$$= \frac{f_B m_B^2 \langle \pi^-(p)\pi^+(-q)|O|B(p-q)\rangle_T}{m_B^2 - (p-q)^2}$$
$$+ \int_{s_h^B}^\infty ds' \frac{\rho_h^{(B)}(s')}{s' - (p-q)^2}, \tag{42}$$

where f_B is the B-meson decay constant. In the ground-state contribution, we have $P^2 = (p-k-q)^2 = m_B^2 + i\epsilon$ and $(p-q)^2 = m_B^2$ simultaneously, so that the artificial momentum k disappears and we encounter the hadronic on-shell matrix element of our interest. After applying the

duality approximation to the integral over excited states in Eq. (42) and performing Borel transformation, we obtain the LCSR for the $B \to \pi\pi$ hadronic matrix element of a given operator and topology:

$$\langle \pi^-(p)\pi^+(-q)|O|B(p-q)\rangle_T$$
$$= \frac{1}{f_B m_B^2 \pi} \int_{m_b^2}^{s_0^B} ds' \, e^{(m_B^2 - s')/M'^2}$$
$$\times \text{Im}_{s'} \Pi_{\pi\pi}^{(O,T)}(s' + i\epsilon, m_B^2 + i\epsilon). \tag{43}$$

Note that the analytical continuations of $\Pi_{\pi\pi}^{(O,T)}$ in the variables s' and P^2 interchange and may be performed in inverse order as well.

V. ANNIHILATION WITH HARD GLUONS

For the correlation function (35) with the operators $O_{1,2}^u$, the simplest possible diagram with the annihilation topology is the factorizable diagram in Fig. 4(a). Its contribution is expected to vanish due to the conservation of the $V - A$ current for massless u, d quarks. In fact, a calculation of the diagram in LCSR yields a parametrically small correction of $O(s_0^\pi/m_B^2)$ which is neglected within the adopted accuracy of the method [13], so that the result is consistent with the expectation.

We start to calculate the annihilation effect by considering the first two $O(\alpha_s)$ diagrams shown in Fig. 4(b); they contain only the operator $\tilde{O}_2^u$. These two-loop diagrams depend on four different mass/momentum scales, m_b, $(p-k)^2$, $(p-q)^2$, and P^2, which makes their direct calculation technically not feasible. As mentioned in the previous section, instead of calculating these diagrams directly, we start from the pion-pion correlator $\Pi_{\pi\pi}^{(\tilde{O}_2^u, A)}$ defined in Eq. (38), with the annihilation topology. The corresponding one-loop diagrams are shown in Fig. 9 and we proceed with their calculation.

After contracting the quark and gluon fields, the long-distance part of $\Pi_{\pi\pi}^{(\tilde{O}_2^u, A)}$, at leading twist 2, reduces to a product of two-pion twist-2 DA's:

$$\langle \pi^-(p-k)|\bar{d}_a^\alpha(z)u_b^\beta(0) \, \bar{u}_c^\gamma(0) d_d^\delta(z)|\pi^-(q)\rangle$$
$$\approx \langle \pi^-(p-k)|\bar{d}_a^\alpha(z)u_b^\beta(0)|0\rangle \cdot \langle 0|\bar{u}_c^\gamma(0)d_d^\delta(z)|\pi^-(q)\rangle$$
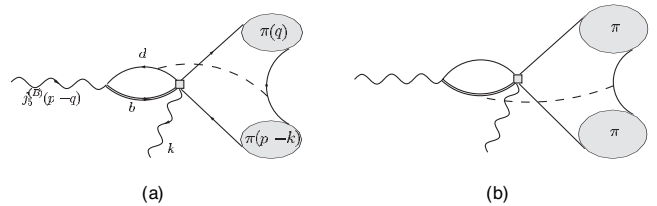

(a)   (b)

FIG. 9.   Diagrams used to calculate the pion-pion correlator in the annihilation topology.

$$= \left(\frac{i\delta_{ab}}{12} f_\pi [(\not p - \not k)\gamma_5]^{\beta\alpha} \int_0^1 dv\, e^{iv(p-k)\cdot z} \varphi_\pi(v)\right)$$

$$\cdot \left(\frac{-i\delta_{cd}}{12} f_\pi [\not q \gamma_5]^{\delta\gamma} \int_0^1 du\, e^{-iuq\cdot z} \varphi_\pi(u)\right),$$

where α, β, γ, δ and a, b, c, d are the spinor and color indices, respectively. Convoluting the above with the short-distance part, one obtains the following expression for the pion-pion correlator :

$$\Pi_{\pi\pi}^{(\tilde{O}_2^u,A)}((p-q)^2, P^2) = -i\left(\frac{\alpha_s C_F}{\pi}\right)\frac{f_\pi^2 m_b^2}{48}$$

$$\times \int_0^1 du \int_0^1 dv \frac{\varphi_\pi(u)\varphi_\pi(v)}{[(p-q)^2 u - P^2 v]^2}$$

$$\times \{H_{\pi\pi}^d(u, v; (p-q)^2, P^2)$$

$$+ H_{\pi\pi}^b(u, v; (p-q)^2, P^2)\}, \qquad (44)$$

where $H_{\pi\pi}^d$ and $H_{\pi\pi}^b$ represent the hard-scattering kernels for the diagrams in Figs. 9(a) and 9(b), with the gluon attached to the d and b quark, respectively. The expressions

for $H_{\pi\pi}^{d,b}$ are given in Appendix B in terms of the standard loop integrals. Evaluated at $(p-q)^2$, $P^2 < 0$, the result for Eq. (44) is real and finite, in particular, the numerators in Eq. (44) cancel at the pole $(p-q)^2 u = P^2 v$. Furthermore, $\Pi_{\pi\pi}^{(\tilde{O}_2^u,A)}$ contains no end-point divergences in the variables u and v. The reason why the integrals remain finite is simple: the gluon in the diagrams in Fig. 9 has a virtuality uvP^2, and remains perturbative unless u or v is close to 0, but this region is suppressed by the end-point behavior of the pion DA's. This convergence is important for justifying the replacement of the initial diagrams in Fig. 4(b). Note that the latter are convergent and perturbative 'by construction,' because they contain one off-shell current instead of the pion DA.

For the sum rule derivation we need the dispersion relation (42) for $\Pi_{\pi\pi}^{(\tilde{O}_2^u,A)}$ in the variable $s' = (p-q)^2$. The expression (44) continued in this variable, (while keeping P^2 negative), has branch cuts at $s' > 0$. The calculation of the imaginary part is straightforward, but involved. The result reads:

$$\text{Im}_{s'} \Pi_{\pi\pi}^{(\tilde{O}_2^u,A)}(s' + i\epsilon, P^2) = if_\pi^2 m_b^2 \left(\frac{\alpha_s C_F}{24}\right) \int_0^1 du \int_0^1 dv \frac{\varphi_\pi(u)\varphi_\pi(v)}{uv(u\,s' - v\,P^2)^3}\left[H_1(u, v; s', P^2) \cdot \Theta(s' - m_b^2) \right.$$

$$\left. + H_2(u, v; s', P^2) \cdot \Theta\left(s' - \frac{m_b^2}{\bar{u}} - v\,P^2\right)\right], \qquad (45)$$

where $\bar{u} = 1 - u$ and

$$H_1(u, v; s', P^2) = uv\,P^2(m_b^2 - s' + v\,P^2)^2 \log\left(\frac{v\,P^2|m_b^2 - \bar{u}s'|}{u\,s'(m_b^2 - s' + v\,P^2)}\right) - \left(1 - \frac{m_b^2}{s'}\right)(u\,s' - v\,P^2)(m_b^2 - u\,s' + v\,P^2)$$

$$\times (u\,s' + v\,P^2) - (u(m_b^2 - u\,s') + v\,P^2)(v\,m_b^2 P^2 + u\,s'(s' - v\,P^2)) \log\left|\frac{s'(u\,m_b^2 + \bar{u}v\,P^2)}{u\,s'^2 + v\,P^2(m_b^2 - u\,s')}\right|,$$

$$H_2(u, v; s', P^2) = -uv\,P^2(m_b^2 - s' + v\,P^2)^2 \log\left(\frac{\bar{u}v\,P^2(m_b^2 - s' + v\,P^2)}{u(s' - v\,P^2)|m_b^2 - \bar{u}s'|}\right) + (u\,s' - v\,P^2)\left(1 - \frac{m_b^2}{\bar{u}(s' - v\,P^2)}\right)$$

$$\times (m_b^2(u\,s' + (1 - 2u)v\,P^2) - 2u(s' - v\,P^2)(u\,s' - v\,P^2)) + (u(m_b^2 - u\,s') + v\,P^2)$$

$$\times (v\,P^2 m_b^2 + u\,s'(s' - v\,P^2)) \log\left|\frac{(s' - v\,P^2)(u\,m_b^2 + \bar{u}v\,P^2)}{\bar{u}(u\,s'^2 + v\,P^2(m_b^2 - u\,s'))}\right|.$$

The expression (45) at negative P^2 contains no singularities within the integration region, and is therefore finite. The two pieces proportional to $\Theta(s' - m_b^2)$ and $\Theta(s' - m_b^2/\bar{u} - P^2 v)$ reflect the two cuts of the diagrams in Fig. 9: the first one corresponds to the on-shell b and $\bar{d}$ quarks emitted at the B-current vertex; the second cut is less trivial and emerges when b and d quark at the weak vertex are on shell.

Finally, according to the procedure explained in the previous section, we analytically continue $\text{Im}_{s'} \Pi_{\pi\pi}^{(\tilde{O}_2^u,A)}$ to the physical timelike point $P^2 = m_B^2 + i\epsilon$, so that this function acquires an imaginary part $\text{Im}_{P^2}\text{Im}_{s'} \Pi_{\pi\pi}^{(\tilde{O}_2^u,A)}$. The imaginary part in (45) naturally originates from the logarithms of $-P^2$, however the complexity of this expression makes their extraction nontrivial. We obtain

$$\text{Im}_{P^2}\text{Im}_{s'} \Pi_{\pi\pi}^{(\tilde{O}_2^u,A)}(s', m_B^2) = i\frac{\pi\alpha_s C_F}{24} f_\pi^2\, m_b^2\, m_B^2(m_b^2 - s' + v\,m_B^2)^2 \int_0^1 du \int_0^1 dv \frac{\varphi_\pi(u)\varphi_\pi(v)}{(u\,s' - v\,m_B^2)^3}$$

$$\times \left[\Theta\left(s' - \frac{m_b^2}{\bar{u}}\right) - \Theta(s' - m_b^2 - v\,m_B^2)\right]. \qquad (46)$$

The existence of nonvanishing imaginary part in P^2 is an important effect we are actually looking for, because in the quark-hadron duality approximation it determines the strong phase of the hadronic matrix element. Importantly, Eq. (46) receives contributions only from the diagram in Fig. 9(a). Physically, the effect corresponds to the d quark from the weak decay of b quark going on shell and annihilating with the spectator $\bar{d}$ quark into a virtual timelike gluon. In the diagram in Fig. 9(b) the gluon is attached to the b quark and such mechanism is forbidden kinematically, hence this diagram has no double imaginary part. We have verified by explicit calculation that an identical result is obtained if one does analytical continuation in P^2 first and only then obtains the dispersion relation in s'.

Our final result for the annihilation contribution with hard gluons in twist-2 approximation is given by the sum rule of the type (43):

$$\langle \pi^- \pi^+ | \tilde{O}_2^u | \bar{B}^0 \rangle_A^{\text{hard}} = \frac{1}{f_B m_B^2 \pi} \int_{m_b^2}^{s_0^B} ds' \, e^{(m_B^2 - s')/M'^2}$$
$$\times \text{Im}_{s'} \Pi_{\pi\pi}^{(\tilde{O}_2^u, A)}(s', m_B^2 + i\epsilon), \qquad (47)$$

where the real and imaginary part are given by the real part of Eq. (45) (with the principal value of the integrals containing complex poles) and by Eq. (46), respectively.

As already mentioned, the LCSR result (47) is finite, due to the fact that the end-point divergence introduced by the gluon propagator $1/uvP^2$ is cancelled by the pion DA's. In the light-cone expansion of the two-pion diagrams in Fig. 9 one formally encounters a contribution proportional to the two twist-3 pion DA's which is divergent. However, one has to keep in mind, that we have used these diagrams only as an effective replacement for the part of the diagrams in the correlation function (35). In this function one of the pions is interpolated by the axial-vector current, which simply does not have a twist-3 component. We conclude that the (twist 3) $\otimes$ (twist 3) contribution to $\Pi_{\pi\pi}^{(\tilde{O}_2^u, A)}$ has no counterpart in the correlation function (35) and hence does not play any role in LCSR.

To complete the calculation of hard-gluon effects, we still need to consider the four diagrams in Fig. 4(c) which belong to the $O(\alpha_s)$ part of the correlation function (35). Note that similar diagrams where $B \to \pi\pi$ annihilation is accompanied by gluons exchanged within the weak vertex, also emerge in QCDF approach. However, they were not included in [3], where only the diagrams analogous to Fig. 4(b) were taken into account. The reason, apart from expected $1/m_b$ suppression, is that in order to describe the two-pion state originating from a quark-antiquark pair, in QCDF one needs an additional long-distance object, a sort of two-pion distribution amplitude, which in the local limit reduces to the pion form factor at timelike momentum transfer m_B^2. In LCSR approach the 'form factorlike' annihilation diagrams in Fig. 4(c) emerge as a part of OPE, hence, no new input is needed. However, the calculation of

these diagrams is not possible with current methods, because they contain two loops and many scales. In fact, in this case one cannot use as a remedy the pion-pion correlator considered above, since the corresponding diagrams still have two loops, even if both pions are described by their DA's. In order to assess this effect, remaining at the one-loop level, we employ a completely different method which is briefly described in the rest of this section.

A new type of correlation function is introduced with an on-shell B meson and a pion, while interpolating the second pion with a current[5]:

$$\Pi_\alpha^{B\pi}(p, k, q) = i \int d^4y \, e^{i(p-k)y}$$
$$\times \langle 0 | T\{ j_{\alpha 5}^{(\pi)}(y), \tilde{O}_2^u(0) \} | B(p - q)\pi^-(q) \rangle.$$
$$(48)$$

We consider the part of this correlation function with quark contractions having annihilation topology and pick up only diagrams with gluon exchange in the weak vertex. They can be obtained from the diagrams in Fig. 4(c) if the interpolating current $j_5^{(B)}$ is replaced by an on-shell B meson. The correlation function (48) factorizes into a product of vacuum-to-pion matrix element (that is, a usual pion DA) and vacuum-to-B matrix element. The latter is expressed via B meson DA's [29,30]. As usual, the external momenta are chosen to provide that the virtual quarks and gluon remain far off shell. For the pion DA we retain only twist 2 (twist 3 vanishes in the chiral limit) whereas the two components $\phi^\pm$ of the B meson DA are taken into account. By writing a dispersion relation in the variable $(p - k)^2$ (in the pion channel), one obtains a sum rule for the $B \to \pi\pi$ matrix element. As a result, we find that all four diagrams vanish, which means that contributions from the ''form factor'' part of the annihilation mechanism starts either at higher twists ≥ 4 and/or at higher orders in α_s and can be neglected.

VI. ANNIHILATION WITH SOFT GLUONS

The gluons exchanged between the initial B-meson and the final quark-antiquark state in the $B \to \pi\pi$ annihilation can also have small virtualities. Diagrams with soft-gluon contributions cannot be directly calculated in QCDF or PQCD, because in this case it is difficult to identify and separate a hard kernel. The soft-gluon nonfactorizable effects should either be neglected (arguing that they are $1/m_b$ suppressed) or modeled by separate nonperturbative parameters. In the LCSR approach the decay amplitude is calculated quite differently, by matching the hadronic dispersion relation to the correlation function. In the latter, the soft (low virtuality) gluons emerge in OPE diagrams, being emitted at short distances and absorbed in the quark-anti-

---

[5]A similar but simpler version of this method was recently applied to $B \to \pi$ form factor in Ref. [27] (see also Ref. [28]).

quark-gluon DA's of the pion. For the emission topology the corresponding diagrams are shown in Fig. 2(c). Their effect, although formally $1/m_b$ suppressed turned out [13] to be of the same order as the $O(\alpha_s)$ effect of nonfactorizable hard gluons calculated from QCDF. On the other hand, the soft-gluon effects for the penguin topology (one of diagrams is shown in Fig. 3(b)] were found suppressed in LCSR [18] with respect to the penguin diagrams with hard gluons, indicating that the role of soft-gluon effects strongly depends on the topology. Here we will calculate the soft-gluon diagrams in the part of the correlation function (35) with annihilation topology.

The two lowest-order diagrams are shown in Figs. 4(d) and 4(e) containing an on-shell gluon emitted from the heavy-light loop and absorbed in the three-particle pion DA. Technically these diagrams are much easier to calculate than the annihilation diagrams with hard gluons in Fig. 4(b) and 4(c). One returns to the original method of [13] and employs the light-cone expansion of the quark propagators in the external gluon field [31]. For the diagram with a gluon emission from the massless d quark we use

$$
\begin{aligned}
S_d(x, 0) &= -i\langle 0|T\{d(x)\bar{d}(0)\}|0\rangle \\
&= \frac{\not{x}}{2\pi^2(x^2)^2} - \frac{1}{16\pi^2 x^2}\int_0^1 dv\, G^{\tau\rho}(vx) \\
&\quad \times (\not{x}\sigma_{\tau\rho} - 4iv x_\tau \gamma_\rho) + \dots,
\end{aligned} \tag{49}
$$

whereas the propagator for the massive b quark is

$$
\begin{aligned}
S_b(0, x) &= -i\langle 0|T\{b(0)\bar{b}(x)\}|0\rangle \\
&= \int \frac{d^4k}{(2\pi)^4} e^{ikx} \frac{\not{k} + m_b}{k^2 - m_b^2} - \int_0^1 dv\, G^{\tau\rho}(vx) \\
&\quad \times \int \frac{d^4k}{(2\pi)^4} e^{ikx} \left[\frac{1}{2} \frac{\not{k} + m_b}{(k^2 - m_b^2)^2} + \frac{\bar{v}x_\tau \gamma_\rho}{k^2 - m_b^2} \right] + \dots
\end{aligned} \tag{50}
$$

In the above $\bar{v} = 1 - v$, $G_{\tau\rho} = \frac{\lambda^a}{2} G_{\tau\rho}^a$ and the fixed-point gauge for the gluon field has been adopted, having in mind that the hard and soft contributions to OPE are individually gauge-invariant. The dots in Eqs. (49) and (50) represent terms with derivatives and higher orders of the gluon field-strength tensor which we neglect. These terms generate pion DA's with twist >4 and multiplicity >3, and their contributions to the sum rule are suppressed by additional powers of the Borel parameter.

In the chiral limit for the light quarks, the contribution of the twist-3 quark-antiquark-gluon pion DA vanishes and the nonvanishing part comes from the twist 4. The four relevant DA's $\tilde{\varphi}_{\parallel, \perp}$ and $\varphi_{\parallel, \perp}$ are defined via vacuum-pion matrix elements:

$$
\langle 0|\bar{u}(0) i\gamma_\mu \tilde{G}_{\alpha\beta}(x_3) d(x_1)|\pi(q)\rangle
$$
$$
= f_\pi \int D\alpha_i\, e^{-iq(x_1\alpha_1 + x_3\alpha_3)} \left[(g_{\mu\alpha} q_\beta - g_{\mu\beta} q_\alpha) \tilde{\varphi}_\perp(\alpha_i) \right.
$$
$$
\left. + q_\mu \frac{z_\beta q_\alpha - z_\alpha q_\beta}{qz} (\tilde{\varphi}_\perp(\alpha_i) + \tilde{\varphi}_\parallel(\alpha_i)) \right], \tag{51}
$$

and the one obtained from the above with $i\gamma_\mu \to \gamma_\mu\gamma_5$, $\tilde{G}_{\alpha\beta} \to G_{\alpha\beta}$, and $\tilde{\varphi}_{\parallel,\perp} \to \varphi_{\parallel,\perp}$. In Eq. (51), $\tilde{G}_{\alpha\beta} = \frac{1}{2}\epsilon_{\alpha\beta\rho\lambda} G^{\rho\lambda}$, $\mathcal{D}\alpha_i = d\alpha_1 d\alpha_2 d\alpha_3 \delta(1 - \alpha_1 - \alpha_2 - \alpha_3)$. The points $x_{1,2}$ are located on the light cone, $x_i = u_i z$, where u_i are arbitrary numbers and $z^2 = 0$ is the light-cone separation.

In our case, due to the choice of external spacelike momenta, the regions of integration over x, y are close to the light cone, but x^2, y^2, $(x - y)^2$ are not exactly lightlike. Therefore, strictly speaking, there is an ambiguity of defining z via x and y in right-hand side (r.h.s.) of Eq. (51). From the point of view of the light-cone OPE, this ambiguity is a higher-twist effect. Indeed, calculating the diagrams for different choices $z = x, y, x - y$ in Eq. (51) one finds that the parts proportional to $z_\alpha/(qz)$ in Eq. (51) and its analog for $\gamma_\mu\gamma_5$ yield negligibly small contributions. Hence, only two DA's $\varphi_\perp$ and $\tilde{\varphi}_\perp$ multiplying the coordinate-independent part of the matrix elements appear in the final answer.

After specifying the propagators and pion DA's, the calculation of the diagrams in Figs. 4(d) and 4(e) is straightforward. The following expression is obtained for the invariant amplitude multiplying $(p - k)_\alpha$ in the correlation function:

$$
\begin{aligned}
F_{\text{soft}}^{(\tilde{O}_2^u, A)} &= \frac{m_b^2 f_\pi}{16\pi^2} \int_0^1 \frac{d\alpha_1}{-P^2\alpha_1 - (p-k)^2(1-\alpha_1)} \\
&\quad \times \int_0^{(1-\alpha_1)} d\alpha_3 \int_0^1 dv \int_0^1 \frac{dx}{m_b^2 - (p-q)^2(1-\alpha_3 v)x} \\
&\quad \times \{ [P^2(1 + 2x\bar{v}) + 3(p-q)^2(1 - 2\bar{v}x)]\varphi_\perp(\alpha_i) \\
&\quad - [P^2(1 - 4x\bar{v}) + 3(p-q)^2]\tilde{\varphi}_\perp(\alpha_i) \}.
\end{aligned} \tag{52}
$$

Following the procedure explained in Section IV, we match the above expression to the dispersion relation in the variable $(p - k)^2$. After applying duality and Borel transformation, we obtain for the corresponding pion-pion correlator:

$$
\begin{aligned}
\Pi_{\pi\pi}^{(\tilde{O}_2^u, A),\text{soft}} &= i\frac{m_b^2}{16\pi^2 P^2} \int_0^{s_0^\pi} ds\, e^{-s/M^2} \int_0^1 d\alpha_3 \\
&\quad \times \int_0^1 dv \int_0^1 \frac{dx}{m_b^2 - (p-q)^2(1-\alpha_3 v)x} \\
&\quad \times ([P^2(1 + 2x\bar{v}) + 3(p-q)^2(1 - 2\bar{v}x)] \\
&\quad \times \varphi_\perp(0, \bar{\alpha}_3, \alpha_3) - [P^2(1 - 4x\bar{v}) \\
&\quad + 3(p-q)^2]\tilde{\varphi}_\perp(0, \bar{\alpha}_3, \alpha_3)) \\
&\quad \times \{1 + O(s_0^\pi/P^2)\},
\end{aligned} \tag{53}
$$

where $\bar{\alpha}_3 = 1 - \alpha_3$ and we neglected terms of $O(s/P^2) < O(s_0^\pi/P^2)$.

The analytical continuation to $P^2 = m_B^2$ is then trivial and we can immediately apply the dispersion relation in the variable $(p - q)^2$, and subsequently, duality and the Borel transformation in the B channel. Our final result for the soft-gluon annihilation contribution to the hadronic matrix element in the leading twist-4 approximation reads

$$\langle \pi^- \pi^+ | \tilde{O}_2^u | \bar{B}^0 \rangle_A^{\rm soft} = i \frac{m_b^2}{16\pi^2 f_B m_B^4} \int_0^{s_0^\pi} ds\, e^{-s/M^2} \int_{m_b^2}^{s_0^B} \frac{ds'}{s'} e^{m_B^2/M'^2 - s'/M'^2} \int_{m_b^2/s'}^1 \frac{du}{u} \int_{1-u}^1 \frac{d\alpha_3}{\alpha_3} \left\{ \left[m_B^2 + 3s' + 2(m_B^2 - 3s') \right. \right.$$

$$\left. \times \frac{m_b^2(u - \bar{\alpha}_3)}{s' u \alpha_3} \right] \varphi_\perp(0, \bar{\alpha}_3, \alpha_3) - \left[m_B^2 + 3s' - 4m_B^2 \frac{m_b^2(u - \bar{\alpha}_3)}{s' u \alpha_3} \right] \tilde{\varphi}_\perp(0, \bar{\alpha}_3, \alpha_3) \left. \right\} \{ 1 + O(s_0^\pi/P^2) \}. \tag{54}$$

In the adopted approximation, this part of the decay amplitude does not contribute to the strong phase.

Finally, adding the hard-gluon and soft-gluon contributions given by Eqs. (47) and Eq. (54), respectively, we complete our calculation of the parameter $r_A^{(\pi\pi)}$ defined in Eq. (25).

VII. FACTORIZABLE ANNIHILATION VIA O_6 OPERATOR

In this section we describe the calculation of the pion scalar form factor defined in Eq. (29). According to Eq. (30), this form factor is needed to estimate the factorizable part of the $B \to \pi\pi$ matrix element of the operator O_6^d with annihilation topology.

In QCDF only part of this contribution was taken into account, namely, the annihilation diagrams with the gluon exchange in the final state [see Figs. 4a,b in Ref. [3]]. Clearly, this is not a complete answer, because the annihilation into two pions via the scalar current starts at zeroth order in α_s. In addition, there are $O(\alpha_s)$ diagrams where a hard gluon is exchanged in the final state at the vertex of the scalar current. All these contributions lie beyond the usual QCDF approximation: being formally $1/m_b$ suppressed, they also do not allow a factorization with a hard kernel. One has to parametrize them with a separate nonperturbative parameter.

We use a different approach, considering the scalar pion form factor $\langle \pi^+(p) \mid \bar{q}q \mid \pi^-(q) \rangle$ $(q = u, d)$ as a separate object and obtaining it from LCSR, following the same method as in [19]. The calculation is done at spacelike momentum transfer $P^2 < 0$, analytically continuing the result to large timelike $P^2 = m_B^2$.

One introduces the correlation function

$$T_\alpha(p, q) = i \int d^4x\, e^{ipx} \langle 0 | T\{ j_{\alpha 5}^{(\pi)}(x) \bar{d}d(0) \} | \pi^-(q) \rangle, \tag{55}$$

where $j_{\alpha 5}^{(\pi)}$ is the same axial-vector current as in Eq. (35). Inserting the complete set of states with the pion and axial meson quantum numbers between the currents in Eq. (55), one obtains for the ground-state pion contribution:

$$T_\alpha^{(\pi)}(p, q) = \frac{i f_\pi F_\pi^S(P^2)}{m_\pi^2 - p^2} p_\alpha. \tag{56}$$

At large spacelike p^2 and $P^2 = (p - q)^2$ the correlation function can be expanded near the light cone and expressed via pion DA's. The OPE starts from the diagram in Fig. 10(a) which corresponds to the soft or end-point mechanism of the pion-to-pion transition. In addition, there is a diagram with quark-antiquark gluon DA's [Fig. 10(b)] and $O(\alpha_s)$ diagrams, some of them shown in Figs. 10(c) and 10(d).

To calculate the leading-order diagram in Fig. 10(a), the free d-quark propagator is inserted and pion quark-antiquark DA's are factorized out. Only the structure proportional to p_α is relevant. In the chiral limit (at $q^2 = m_\pi^2 = 0$) the twist-2 contribution vanishes, hence the expansion starts from the twist 3. The answer reads:
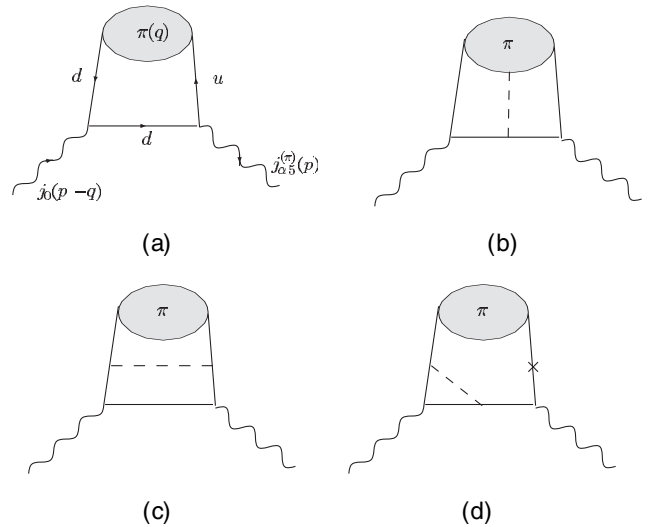

FIG. 10. Diagrams of the correlation function used to derive LCSR for the pion scalar form factor; $j_0 = \bar{d}d$ is the scalar quark current.

$$T_\alpha(p,q) = i\mu_\pi f_\pi \int_0^1 \frac{du}{-p^2 u - P^2 \bar{u}} (\varphi_P(u)$$
$$- \frac{1}{6} \frac{d}{du} \varphi_\sigma(u)) p_\alpha, \qquad (57)$$

where $\varphi_{P,\sigma}$ are the standard twist-3 DA's of the pion, normalized to $\mu_\pi = m_\pi^2/(m_u + m_d)$. In addition, we find that the diagram in Fig. 10(b), with a low-virtuality (soft) gluon absorbed in the quark-antiquark-gluon DA , does not contribute to the relevant Lorentz structure $\sim p_\alpha$ in the chiral limit.

Furthermore, the experience with the LCSR for the pion vector (e.m.) form factor [19] tells that even at rather large momentum transfers of a few GeV^2 the $O(\alpha_s)$ diagrams in Fig. 10(c) and 10(d) are subdominant. Therefore, in what follows we simplify our calculation neglecting their contributions.

Equating the result (57) for the correlation function to the hadronic dispersion relation in the variable p^2, we retain only the pion contribution (56) and replace the sum over heavier states by a quark-hadron duality estimate. For that one has to write the expression (57) as a dispersion relation in the variable $s = p^2 > 0$ by substituting the integration variable: $u = -P^2/(s - P^2)$. After Borel transformation we obtain the LCSR for the pion scalar form factor valid at large spacelike $P^2 < 0$. Continuing it to large timelike $P^2 = m_B^2$, we get

$$F_\pi^S(m_B^2) = -\frac{\mu_\pi}{m_B^2} M^2 (1 - e^{-s_0^\pi/M^2})$$
$$\times \left(\varphi_P(u) - \frac{1}{6} \frac{d}{du} \varphi_\sigma(u) \right) \Big|_{u=1}$$
$$\times (1 + O(s_0^\pi/m_B^2)) \qquad (58)$$

with an evident end-point dominance. Note that $F_\pi^S(m_B^2)$ has no imaginary part in the adopted approximation. It will appear at $O(\alpha_s)$, hence, we expect the strong phase in the form factor to be subdominant.

Substituting Eq. (58) in Eq. (30), we obtain the estimate for the parameter $R_A^{(\pi\pi,6)}$. Containing a chiral enhanced factor, and having no α_s suppression, this effect is expected to be important. On the other hand, the annihilation effects via $O_{5,6}$ operators multiply small Wilson coefficients c_5 and c_6 in the amplitude (27), therefore in what follows we only retain $R_A^{(\pi\pi,6)}$ and neglect nonfactorizable corrections parametrized by $r_A^{(\pi\pi,6)}$ and $r_A^{(\pi\pi,5)}$.

VIII. NUMERICAL ESTIMATES

For the numerical evaluation we adopt the same input in all sum rules derived and used in this paper, including LCSR (47) and (54), and (58) for the matrix elements in the annihilation topology, and the LCSR for the $B \to \pi$ form factor $f_{B\pi}^+$ [16] determining the factorizable amplitude $\mathcal{A}_{\pi\pi}$. Finally, f_B is substituted by the corresponding

two-point sum rule, so that the uncertainties of the input parameters partly cancel in the ratios.

In the LCSR for $B \to \pi$ form factor [16] the one-loop pole mass m_b of the b quark is used. For consistency, we adopt the same mass for the other sum rules. The current interval $\bar{m}_b(\bar{m}_b) = 4.25 \pm 0.15$ GeV [32] converted into the one-loop pole mass yields $m_b = 4.7 \pm 0.1$ GeV. Furthermore, we take $\alpha_s(m_Z) = 0.1187$ [32], evolved to lower scales at two-loop order, so that e.g., $\alpha_s(m_b/2) = 0.284$. For the factorization and renormalization scale of the scale-dependent input parameters, we use $\mu_b = \sqrt{m_B^2 - m_b^2} \simeq 2.4$ GeV, numerically close to $m_b/2$. Being of order of the Borel parameter M' in the B-meson channel, this scale reflects the average virtuality in the correlation function. For consistency, we normalize also the Wilson coefficients in H_{eff} at the same scale μ_b. For the latter, we use the NLO results obtained in the NDR scheme adopted in our calculation:

μ	c_1	c_2	c_3	c_4	c_5	c_6	c_{8g}
2.4 GeV	1.124	-0.272	0.020	-0.037	0.010	-0.060	-0.166
4.8 GeV	1.073	-0.174	0.013	-0.034	0.009	-0.038	-0.149

In our uncertainty estimates, we include the variation of the unified scale up to $2\mu_b$.

Furthermore, for the condensate densities used in the sum rules, we take $\langle \bar{q}q \rangle (1 \text{ GeV}) = (-0.240 \pm 0.010 \text{ GeV})^3$, so that $\mu_\pi(1 \text{ GeV}) = 1.61 \pm 0.20$ GeV; $\langle \frac{\alpha_s}{\pi} G^2 \rangle = 0.012 \pm 0.006 \text{ GeV}^4$ and $\langle \bar{q}Gq \rangle = (0.8 \pm 0.2 \text{ GeV}) \times \langle \bar{q}q \rangle (1 \text{ GeV})$, the scale dependence of the quark-gluon condensate density being negligible. The remaining parameters in the B channel are: the interval of the Borel parameter $M'^2 = 10 \pm 2 \text{ GeV}^2$ and the duality threshold $s_0^B = 35 \mp 2 \text{ GeV}^2$ chosen as in [13]. Concerning the parameters related to the pion, we use the experimental value $f_\pi = 131$ MeV [32], and take the Borel interval $M^2 = 1.0^{+0.5}_{-0.2} \text{ GeV}^2$ as well as the duality threshold $s_0^\pi = 0.7 \text{ GeV}^2$ determined from the two-point sum rule for f_π [15].

Finally, the pion light-cone DA's deserve a separate discussion. Their definitions, asymptotic forms, and non-asymptotic parts used in our calculation can be found, e.g., in Appendix B of Ref. [20].

In the twist-2 pion DA $\varphi_\pi(u)$, we include nonasymptotic effects encoded by the Gegenbauer moments a_2^π and a_4^π. These parameters have recently been estimated in Ref. [33] by fitting the LCSR result for $B \to \pi$ form factor to the data on $B \to \pi l \nu$ decay distribution:

$$a_2^\pi(1 \text{ GeV}) = 0.1 \pm 0.1, \quad a_4^\pi(1 \text{ GeV}) \geq -0.07. \qquad (59)$$

We combine this range with the constraint [34] obtained from the analysis of the $\pi \gamma^* \gamma$ form factor

$$a_2^\pi(1 \text{ GeV}) + a_4^\pi(1 \text{ GeV}) = 0.1 \pm 0.1. \qquad (60)$$

The resulting intervals

$$a_2^\pi(1\ \text{GeV}) = 0 \div 0.27,$$
$$a_4^\pi(1\ \text{GeV}) = -0.07 \div 0.20, \tag{61}$$

are consistent with other estimates in the literature. Note that Eq. (61) does not exclude a purely asymptotic DA. Both Gegenbauer moments are independently varied around middle values of the intervals (61) to estimate the corresponding uncertainty. Finally, for the twist-3 and 4 pion DA's, the normalization constants and nonasymptotic parameters are taken as: $f_{3\pi}(1\ \text{GeV}) = 0.0035 \pm 0.0018\ \text{GeV}^2$, $\omega_{3\pi}(1\ \text{GeV}) = -2.88$ and $\delta_\pi(1\ \text{GeV}) = 0.17 \pm 0.05\ \text{GeV}^2$, $\epsilon_\pi(1\ \text{GeV}) = 0.5$, respectively.

Using the input specified above, we reevaluate the result of [35] for the $B \to \pi$ form factor:

$$f_{B\pi}^+(0) = 0.26 \pm 0.02_{[a_{2,4}^\pi]} \pm 0.03_{[\text{param}]}, \tag{62}$$

where the uncertainties induced by Gegenbauer moments and by other sum rule parameters (the latter are added up in quadrature) are shown separately. This estimate agrees well with the most recent calculation of this form factor in Ref. [36] where also a small twist-3 NLO correction is taken into account. In Section II we added both uncertainties linearly to be on the conservative side. In what follows, all errors are added quadratically.

Using the sum rules for hard- and soft-gluon contributions presented in Sections V and VI, we first estimate the ratio $r_A^{(\pi\pi)}$. We find that both hard-gluon and soft-gluon annihilation contributions, being comparable in magnitude, are numerically very small and partly cancel each other, so that

$$r_A^{(\pi\pi)} = [-0.67^{+0.47}_{-0.87} + i(3.6^{+0.5}_{-1.1})] \times 10^{-3}. \tag{63}$$

On the other hand, the factorizable annihilation via quark-penguin operator O_6 produces a considerably larger hadronic matrix element:

$$R_A^{(\pi\pi,6)} = 0.23^{+0.05}_{-0.08}. \tag{64}$$

However, the small Wilson coefficient reduces the effect in the decay amplitudes to the same level as for the annihilation via the current-current operator: $(c_6 + c_5/3)R_A^{(\pi\pi,6)} \sim c_1 r_A^{(\pi\pi)}$. As mentioned at the end of Section VII, we therefore neglect both factorizable and nonfactorizable $O(\alpha_s)$ corrections to the annihilation via the operators O_5 and O_6. In general, the contributions of annihilation amplitudes are found at the same level as the other nonfactorizable effects estimated from LCSR in Refs. [13,17,18].

Having at hand the new estimates of $r_A^{(\pi\pi)}$ and $R_A^{(\pi\pi,6)}$, we now update the phenomenological analysis of $B \to \pi\pi$ channels, with all nonfactorizable parts of the amplitudes calculated from LCSR, except the emission with hard gluons which is estimated using QCDF. To this end, we recalculated the previous LCSR predictions using the current input, which has only slightly changed. For the non-factorizable emission, we obtain

$$r_E^{(\pi\pi)} = [(1.8^{+0.5}_{-0.7}) \times 10^{-2}]_{\text{soft}} + [(1.3^{+5.6}_{-5.2}) \times 10^{-2}$$
$$+ i(-4.7^{+1.1}_{-0.3}) \times 10^{-2}]_{\text{hard}}, \tag{65}$$

where the soft-gluon part is obtained from [13] and the hard-gluon contribution is estimated using QCDF [2,3] with the default value and error for the parameter describing the twist-3 hard-spectator diagrams. For the quark-penguin operators with scalar-pseudoscalar Dirac structure, we have found that the soft-gluon emission contribution vanishes in twist ≤ 4, and for the hard-gluon part we again use QCDF:

$$r_E^{(\pi\pi,6)} = [(-2.7 \pm 0.4) \times 10^{-2}]_{\text{hard}}. \tag{66}$$

The penguin-topology effects are calculated from LCSR obtained in Refs. [17,18]. The resulting ratios to the factorizable amplitude are:

$$r_{P_q}^{(\pi\pi)} = [0.11^{+0.02}_{-0.36} + i(1.1^{+0.2}_{-0.1})] \times 10^{-2},$$
$$r_{P_c}^{(\pi\pi)} = [-0.18^{+0.06}_{-0.68} + i(-0.80^{+0.17}_{-0.08})] \times 10^{-2},$$
$$r_{P_b}^{(\pi\pi)} = (0.93^{+0.09}_{-0.65}) \times 10^{-2},$$
$$r_{8g}^{(\pi\pi)} = -(3.8^{+1.3}_{-0.4}) \times 10^{-2}, \tag{67}$$

and the modified penguin parameters are $\bar{r}_{P_{q,c,b}}^{(\pi\pi)} \simeq r_{P_{q,c,b}}^{(\pi\pi)} - (\alpha_s C_F)/(36\pi)$; for brevity we do not show the corresponding numbers.

Having specified all parameters entering the decomposition of $B \to \pi\pi$ amplitudes in Eqs. (20) and (21), we calculate the branching ratios and direct CP asymmetries, using the values of B meson lifetimes from [21], and the relevant CKM parameters from [23]. In particular, we adopt $|V_{ub}| = (4.22 \pm 0.26) \cdot 10^{-3}$ (the errors added in quadrature) and use a representative interval $\gamma = (58.6 \pm 10)°$. The results are:

$$BR(B^+ \to \pi^+\pi^0) = (6.7^{+1.8+0.9}_{-1.5-0.8}) \times 10^{-6},$$
$$BR(B^0 \to \pi^+\pi^-) = (9.7^{+2.3+1.2}_{-1.9-1.2}) \times 10^{-6}, \tag{68}$$
$$BR(B^0 \to \pi^0\pi^0) = (0.29^{+0.24+0.07}_{-0.12-0.07}) \times 10^{-6},$$

where the errors represent the variation of the LCSR parameters and of the CKM factors, respectively. The direct CP asymmetries are presented in Table I. For completeness, we also calculate the amplitudes T, P, and C defined in (34) parametrizing them as in [5]:

$$xe^{i\Delta} = \frac{C_{\pi\pi}}{T_{\pi\pi}}, \qquad de^{i\Theta} = -\frac{P_{\pi\pi}}{T_{\pi\pi}}. \tag{69}$$

We obtain:

TABLE I.   Direct *CP* asymmetries from experiment (all numbers taken from [21]; the errors added in quadrature) compared with the LCSR predictions.

	$a_{CP}^{\text{dir}}(B^+ \to \pi^+ \pi^0)$	$a_{CP}^{\text{dir}}(B^0 \to \pi^+ \pi^-)$	$a_{CP}^{\text{dir}}(B^0 \to \pi^0 \pi^0)$
BABAR	-0.01 ± 0.10	0.09 ± 0.16	0.12 ± 0.56
Belle	0.02 ± 0.08	0.56 ± 0.14	0.44 ± 0.56
Average	0.01 ± 0.06	0.37 ± 0.10	0.28 ± 0.40
This work	0	$-0.04 \pm 0.01 \pm 0.01$	$-0.70^{+0.19+0.08}_{-0.29-0.08}$

$$x = 0.29^{+0.15}_{-0.09}, \qquad \Delta = (-21^{+9}_{-7})°,$$
$$d = 0.22^{+0.02+0.01}_{-0.03-0.01}, \qquad \Theta = (-173 \pm 1)°, \tag{70}$$

where the second error in d stems from the uncertainty of $|V_{ub}|$.

We find that the general picture does not qualitatively deviate from the naive factorization considered in Section II. Although the nonfactorizable contributions substantially enhance the small $B^0 \to \pi^0 \pi^0$ amplitude predicted in naive factorization, the disagreement between theory and experiment for the branching ratio of this decay remains. Our prediction (70) for the amplitudes is inconsistent with the fit [5] to data. As already discussed in Section II, one possible interpretation of this disagreement is a missing contribution to the $I = 0$ parts of the amplitudes $T_{\pi\pi}$, $C_{\pi\pi}$, and $P_{\pi\pi}$.

IX. COMPARISON WITH QCD FACTORIZATION

Let us first investigate the behavior of the annihilation amplitudes obtained from LCSR in the heavy quark limit, by making standard substitutions in the sum rules:

$$m_B = m_b + \bar\Lambda, \qquad s_0^B = m_b^2 + 2m_b\omega_0,$$
$$M'^2 = 2m_b\tau, \qquad f_B = \hat f_B / \sqrt{m_b}, \tag{71}$$

where $\bar\Lambda$, ω_0, τ, and $\hat f_B$ are m_b-independent parameters.[6] At $m_b \to \infty$, the factorizable amplitude $\mathcal{A}_{\pi\pi}$ defined in Eq. (12) scales as $m_b^{1/2}$. Expanding in $1/m_b$ the annihilation contribution with hard gluons given by Eq. (47) and dividing it by $\mathcal{A}_{\pi\pi}$, we reduce the real part of the diagram in Fig. 9(a) (gluon emitted by the light quark) to

$$r_{A,\text{hard}}^{(\pi\pi)} \sim \frac{\Lambda}{m_b} \int_0^1 du \frac{\varphi_\pi(u)}{u^2} \int_0^1 dv \frac{\varphi_\pi(v)}{v} + \cdots, \tag{72}$$

where Λ is a generic energy scale not related to m_b and higher powers in $1/m_b$ are denoted by ellipses. Although formally suppressed by $1/m_b$, this expression recovers the logarithmic divergence at $u \to 0$, of the annihilation contribution in QCDF. Importantly, in LCSR this divergence occurs only at $m_b \to \infty$. Moreover, as the numerical analy-

sis in Section VIII shows, at finite $m_b \sim 5$ GeV the logarithms originating from the end-point region (at $m_b \to \infty$ they reduce to $\text{Log}(m_b/\tau)$ and $\text{Log}(m_b/\omega)$) do not produce an enhancement of the annihilation contribution. Furthermore, analyzing LCSR in the heavy quark limit, we observe that the phase generated by the diagram in Fig. 9(a), as well as the contribution of the gluon emission from the heavy quark [Fig. 9(b)], remain finite at $m_b \to \infty$, being of the same $O(1/m_b)$. Other contributions that we have calculated from LCSR, the soft-gluon part of $r_A^{(\pi\pi)}$, and the factorizable annihilation with O_6 given by $R_A^{(\pi\pi,6)}$, are also finite, being suppressed by an additional power of $1/m_b$ with respect to Eq. (72).

The origin of the end-point divergence in QCDF and the reason why it is absent in the LCSR approach can be readily understood. The power counting in QCDF implies that the momentum of the light quark in the B meson has to vanish, i.e. the propagator of the light quark shrinks to a point [2,3]. This is different in LCSR, since the B meson is effectively replaced by the spectral density of the heavy-light-quark loop integrated over the duality interval $m_b^2 < s' < s_0^B$, and thus the momentum of the light quark is nonvanishing. In other words, the end-point singularity is regularized by the typical momentum of the light quark.

To demonstrate this, let us slightly modify QCDF by convoluting the annihilation hard kernels with the standard B-meson DA. We consider the annihilation diagrams in Fig. 9, where instead of the current $j_5^{(B)}$, an on-shell B meson is inserted, represented by its DA. The result for the annihilation amplitude A_1^i (see the definition in [3]) in the twist-2 approximation reads:

$$A_1^i = \pi\alpha_s \int_0^\infty d\omega\, \phi_B^+(\omega) \int_0^1 du\, \varphi_\pi(u) \int_0^1 dv\, \varphi_\pi(v)$$
$$\times \left[\frac{1}{\bar u v(\bar u - \omega/m_B)} \right.$$
$$\left. + \frac{\bar u + \omega/m_B}{\bar u v(1 - (u - \omega/m_B)(\bar v - \omega/m_B))} \right], \tag{73}$$

where the B-meson DA $\phi_B^+(\omega)$ is normalized as: $\int_0^\infty d\omega\, \phi_B^+(\omega) = 1$. Neglecting the spectator quark momentum ω, that is, replacing $\phi_B^+(\omega) \to \delta(\omega)$, one recovers the expression for A_1^i given in [2,3] (see also [38]), with an end-point divergence in the first term in brackets (corresponding to the diagram with gluon emission from the light

---

[6]Note that the scale τ has to be large in comparison with Λ_{QCD}, allowing one to use the power expansion in $\Lambda_{\text{QCD}}/\tau$, so that QCD sum rules remain valid in the heavy quark limit (the well-known example is the sum rule for f_B in HQET [37]).

quark). However, it is generally expected (see e.g., [30]) that $\phi_B^+(\omega) \to 0$ at $\omega \to 0$. The integral in Eq. (73) then converges (taken as a principal value) yielding $\mathrm{Log}(m_B/\lambda_B)$, λ_B being the size of the region in ω where the function $\phi_B^+(\omega)$ dominates. Simultaneously, this expression acquires an imaginary part,[7] due to the pole in the integration region at $\bar{u} = \omega/m_B$.

Employing a realistic model of $\phi_B^+(\omega)$, e.g., the one suggested in [30]:

$$\phi_B^+(\omega) = \frac{\omega}{\lambda_B^2} e^{-\omega/\lambda_B}, \qquad (74)$$

it is easy to calculate Eq. (73) numerically and to estimate the corresponding parameter $r_A^{(\pi\pi)}$ (see Appendix A for the relation between this parameter and A_1^i). The result turns out small, with both real and imaginary parts at the level of $\sim 1\%$, that is, roughly of the same size as the LCSR estimate obtained in the previous section. The model of annihilation represented by Eq. (73) is rather crude, because the transverse momenta of the quarks in B meson are neglected, but their account could not qualitatively change the result. Thus, from the point of view of the LCSR approach, the end-point divergence in the annihilation diagrams in QCDF originates in the hard-scattering approximation and the $m_b \to \infty$ limit.

In the phenomenological analysis of $B \to \pi\pi$ done in Ref. [3], a model for the annihilation diagrams was used, replacing all divergent integrals by a generic logarithm:

$$\int_0^1 \frac{dy}{y} \to X_A = (1 + \rho_A e^{i\varphi_A}) \ln\frac{m_b}{\Lambda_h}, \qquad (75)$$

where $\Lambda_h = 0.5$ GeV, $\rho_A < 1$ and the phase φ_A is arbitrary. With this model the effective annihilation coefficients $(\mathcal{B}_{\pi\pi}/\mathcal{A}_{\pi\pi})b_i$, (where $\mathcal{B}_{\pi\pi} = i(G_F/\sqrt{2})f_B f_\pi^2$) entering the decay amplitudes have been estimated [3]. Using our results and the relations given in Appendix A, we can also obtain these coefficients:

$$\frac{\mathcal{B}_{\pi\pi}}{\mathcal{A}_{\pi\pi}} b_1 = [-0.15^{+0.11}_{-0.19} + i(0.82^{+0.11}_{-0.27})] \times 10^{-2},$$

$$b_2 = \frac{c_2}{c_1} b_1,$$

$$\frac{\mathcal{B}_{\pi\pi}}{\mathcal{A}_{\pi\pi}} b_3 = [-1.3^{+0.7}_{-0.3} + i(0.015^{+0.002}_{-0.008})] \times 10^{-2}, \qquad (76)$$

$$b_4 \simeq \frac{c_4}{c_1} b_1.$$

The above estimates, especially for b_1, differ from the ones presented in [3] for the default value $\rho_A = 0$ in Eq. (75). In fact, a numerical agreement is not anticipated, because the two sets of b_i's originate from two different methods.

---

[7]The appearance of an imaginary part due to the momentum of spectator quark was noticed already in [6] while discussing the differences between QCDF and PQCD.

Moreover, one cannot expect that LCSR predictions for b_i allow a parametrization with a single complex parameter X_A. Important is that both the default values of the annihilation coefficients in [3] and our predictions in Eq. (76) are very small in comparison with the factorizable amplitude. Hence, LCSR is in a qualitative agreement with QCDF, if the annihilation effects in the latter are represented by moderate logarithms.

To complete the comparison with other methods, let us briefly discuss PQCD [6]. In this approach, all $B \to \pi\pi$ amplitudes as well as the $B \to \pi$ form factor are represented by the diagrams with $O(\alpha_s)$ hard-scattering kernels and meson wave functions. Another distinctive feature of PQCD concerns nonvanishing transverse momenta of partons in mesons, which can only be introduced in a model-dependent way. Hence, the annihilation amplitudes in this approach are protected from the end-point divergences and acquire imaginary parts. There is however a basic difference between LCSR and PQCD approaches to $B \to \pi\pi$. In LCSR the diagrams at $O(\alpha_s)$ are subleading and numerically suppressed, justifying the perturbative expansion within OPE. Moreover, the higher-twist soft-gluon diagrams of $O(1/m_b)$ are as important as the $O(\alpha_s)$ effects. Importantly, the dominant part of the $B \to \pi$ form factor in LCSR is soft and has no relation to α_s. In PQCD, the whole form factor (hence, the factorizable part of the $B \to \pi\pi$ amplitude) is assumed to be of $O(\alpha_s)$. Furthermore, the main contribution to the strong phase in PQCD stems from the annihilation mechanism with the scalar-pseudoscalar operator O_6, and the diagrams again start at $O(\alpha_s)$ level. We have also found O_6 to be an important source of factorizable annihilation, but in LCSR the $O(\alpha_s)$ contribution to this mechanism is expected to be subleading in comparison with the zeroth order in α_s, soft contribution which has been calculated in Section VII. Starting at $O(\alpha_s)$ level and neglecting soft contributions, PQCD nevertheless predicts annihilation effects that are larger then in LCSR. This surprising fact means that it is difficult if not impossible to reconcile these two approaches with each other.

X. CONCLUSION

In this paper, the weak annihilation contributions to $B \to \pi\pi$ decay amplitudes have been calculated applying the method of LCSR. This work complements previous studies [13,17,18,39] of nonfactorizable effects in $B \to \pi\pi$ with the QCD sum rule approach. In LCSR, due to sufficient virtuality of the underlying correlation function, the OPE diagrams with annihilation topology are free from end-point divergences. Both contributions of hard and soft gluons are taken into account. A finite result for the hadronic matrix element of the current-current O_1^u operator with annihilation topology is obtained including an imaginary part which contributes to the strong phase. In addition, an important factorizable contribution from the quark-penguin operator O_6 has been found. For the annihilation

with hard gluons considered in this paper, we have modified the method suggested in [13], to avoid the problem of calculating two-loop multiscale diagrams. Instead of performing the QCD calculation based on the vacuum-to-pion correlation function, we start from the pion-pion correlator, thereby reducing the calculation to one-loop diagrams.

We emphasize that QCD sum rules have a limited accuracy, at the same time one is able to estimate the uncertainties of the method. Moreover, many uncertainties cancel in the ratios of nonfactorizable and factorizable hadronic matrix elements obtained from LCSR. Obtaining $B \to \pi\pi$ hadronic matrix elements one uses an additional assumption of the local quark-hadron duality, allowing the transition (analytical continuation) from a large spacelike scale to the large timelike scale m_B^2. This approach has much in common with evaluating the timelike asymptotics of the pion e.m. form factor from the QCD calculation in the spacelike region.

Our main phenomenological result is a smallness of the annihilation contributions in $B \to \pi\pi$. This is generally consistent with QCDF, if the divergent annihilation diagrams there are modeled by moderate logarithmic factors. Hence, we find no compelling reason to consider the annihilation amplitude as a free parameter in QCDF. The relatively large values of this parameter generated by the fits to the data are probably not originating from the annihilation mechanism.

Small annihilation effects predicted in this paper are in the same ballpark as other nonfactorizable contributions obtained from LCSR, including charming and gluonic penguin topologies and nonfactorizable corrections to the emission topology. Altogether, the smallness of the corrections to the leading-order factorizable amplitude reveals a good convergence of the OPE series for the correlation function and justifies the use of the adopted approximation in LCSR, that is, including only $O(\alpha_s)$ and twists ≤ 4, as well as omitting the small $O(s_0^\pi/m_B^2)$ corrections in each term of OPE.

Furthermore, we have performed the phenomenological analysis of the three $B \to \pi\pi$ channels using the results of LCSR for all nonfactorizable effects, except the hard-gluon nonfactorizable corrections to the emission topology. For the latter the default prediction of QCDF [2,3] is used. Our results disagree with the current data for $BR(B^0 \to \pi^+\pi^-)$ and $BR(B^0 \to \pi^0\pi^0)$ and probably also for the direct *CP* asymmetry in $B^0 \to \pi^+\pi^-$, that is, for the channels where the $\Delta I = 1/2$ weak transition (or, equivalently, the $I = 0$ two-pion final state) contributes. If the experimental data do not change, we have to admit that LCSR misses an important part of the isoscalar amplitude. Then a new "inverse $\Delta I = 1/2$" rule has to be established for these decays, meaning that the amplitude A_0 introduced in Section II has to decrease after including the missing piece.

A natural question arises: are there additional mechanisms in $B \to \pi\pi$ which may fill this gap. The penguin-

annihilation topology comes first to one's mind, a possibility which was not yet explored by both QCDF and LCSR. This effect contains multiloop diagrams and cannot be easily evaluated. Still, the experience with LCSR for charming penguins [18] tells us that the OPE diagrams of the type shown in Fig. 5 could not be large. In any case, the penguin-annihilation mechanism deserves a closer look in future. One can for example speculate about nonperturbative gluonic effects in this mechanism, which have an anomalously large scale ($\gg \Lambda_{QCD}$) and lie beyond OPE. Such effects will most probably influence other neutral final states, e.g., enhance $B \to \rho^0\rho^0$. That however seems not to be the case because the current experimental upper bound for $BR(B \to \rho^0\rho^0)$ is less than the measured value of $BR(B \to \pi^0\pi^0)$.

Another resource of enhancement is the hard-spectator part in the nonfactorizable emission. The corresponding diagrams in QCDF diverge at twist 3 and are replaced by another generic logarithm. In our numerical estimates we have taken the default value of this parameter from [3], but the fits to the current data [4] with a free parameter for this contribution produce large effects. Indications that the hard-spectator mechanism is important, were found recently in the SCET framework [40]. We plan to study the nonfactorizable hard-gluon emission, including the hard-spectator mechanism in LCSR (work in progress).

Finally, an important avenue of future studies is the sum rule analysis of the $B \to \pi K$ and $B \to K\bar{K}$ channels including calculable $SU(3)$ violation effects which are expected [39] to be important. The variety of kaon channels with a lot of accumulated data will allow to isolate various topologies, and to put the LCSR approach under a tighter scrutiny.

ACKNOWLEDGMENTS

APPENDIX A: EFFECTIVE COEFFICIENTS IN QCDF

For convenience, we present here the relations between the nonfactorizable matrix elements parametrized in Section III by the ratios $r_T^{(\pi\pi)}$ and the effective coefficients a_i introduced in [2,3] for $B \to \pi\pi$. The decay amplitudes written in terms of these coefficients are:

$$A(\bar{B}^0 \to \pi^+\pi^-) = [\lambda_u a_1 + \sum_{p=u,c} \lambda_p (a_4^p + r_\chi^\pi a_6^p)] \mathcal{A}_{\pi\pi}$$

$$+ [\lambda_u b_1 + (\lambda_u + \lambda_c)(b_3 + 2b_4)] \mathcal{B}_{\pi\pi},$$

$$\sqrt{2} A(B^- \to \pi^-\pi^0) = \lambda_u(a_1 + a_2) \mathcal{A}_{\pi\pi}, \tag{A1}$$

where $r_\chi^\pi = 2\mu_\pi/m_b$ and electroweak penguins are neglected. Comparing with Eqs. (20), (21), (23), (24), and (26), and (27) we obtain:

$$a_1 = c_1 + \frac{c_2}{3} + 2c_2 r_E^{(\pi\pi)},$$

$$a_2 = c_2 + \frac{c_1}{3} + 2c_1 r_E^{(\pi\pi)}, \tag{A2}$$

$$a_4^p + r_\chi a_6^p = c_4 + \frac{c_3}{3} + 2c_3 r_E^{(\pi\pi)} + 2c_1 r_{P_u}^{(\pi\pi)} + 2c_3(r_{P_u}^{(\pi\pi)}$$

$$+ r_{P_b}^{(\pi\pi)}) + 2(c_4 + c_6)(3\bar{r}_{P_q}^{(\pi\pi)} + \bar{r}_{P_c}^{(\pi\pi)} + \bar{r}_{P_b}^{(\pi\pi)})$$

$$+ r_\chi^\pi \left(c_6 + \frac{c_5}{3}\right) + 2c_5 r_E^{(\pi\pi,6)} + c_{8g}^{\text{eff}} r_{8g}^{(\pi\pi)},$$

$$b_1 = 2c_1 r_A^{(\pi\pi)} \frac{\mathcal{A}_{\pi\pi}}{\mathcal{B}_{\pi\pi}},$$

$$b_3 = \left[2c_3 r_A^{(\pi\pi)} + \left(c_6 + \frac{c_5}{3}\right) R_A^{(\pi\pi,6)} + 2c_5 r_A^{(\pi\pi,6)}\right] \frac{\mathcal{A}_{\pi\pi}}{\mathcal{B}_{\pi\pi}},$$

$$b_4 = 2[c_4 r_A^{(\pi\pi)} + c_6 r_A^{(\pi\pi,5)}] \frac{\mathcal{A}_{\pi\pi}}{\mathcal{B}_{\pi\pi}}. \tag{A3}$$

The correspondence between the annihilation diagrams introduced in [3] and parameters $r_A^{(\pi\pi)}$ is schematically given by

$$r_A^{(\pi\pi)} \mathcal{A}_{\pi\pi} \overset{\wedge}{=} \frac{C_F}{18} A_1^i \mathcal{B}_{\pi\pi}, \qquad r_A^{(\pi\pi,5)} \mathcal{A}_{\pi\pi} \overset{\wedge}{=} \frac{C_F}{18} A_2^i \mathcal{B}_{\pi\pi},$$

$$R_A^{(\pi\pi,6)} \mathcal{A}_{\pi\pi} \overset{\wedge}{=} \frac{C_F}{3} A_3^f \mathcal{B}_{\pi\pi}, \qquad r_A^{(\pi\pi,6)} \mathcal{A}_{\pi\pi} \overset{\wedge}{=} \frac{C_F}{18} A_3^i \mathcal{B}_{\pi\pi}, \tag{A4}$$

where the sign $\overset{\wedge}{=}$ indicates that in LCSR and QCDF different approximations are used to calculate left-hand side (l.h.s.) and r.h.s., respectively. In particular, $R_A^{(\pi\pi,5)}$ is of the zeroth order in α_s, whereas A_3^f is of $O(\alpha_s)$.

APPENDIX B: KERNELS FOR HARD ANNIHILATION

The kernels for the hard annihilation contribution to the correlation function in Eq. (44) are given by

$$H_{\pi\pi}^d(u, v; s' = (p - q)^2, P^2) = [P^2(2m_b^2 - s'(2 + u) + 3P^2 v)]B_0(P^2 uv, 0, 0) - \left[\frac{1}{uv}((s'u + P^2 v)m_b^2 + 2P^4 v^2 - s'^2 u\right.$$

$$\left. - P^2 s' v\right]B_0(s', 0, m_b^2) + \left[\frac{1}{uv}((s'u + P^2 v(1 - 2u))m_b^2 + P^4 v^2(1 - 3u) - s'^2 u(1 + u)\right.$$

$$\left. + vP^2 s'(u^2 + 4u - 1))\right]B_0((1 - u)(s' - P^2 v), 0, m_b^2) + [2P^2(m_b^2 - s' + P^2 v)^2]$$

$$\times C_0(s', P^2 uv, (1 - u)(s' - P^2 v), m_b^2, 0, 0),$$

$$H_{\pi\pi}^b(u, v; s' = (p - q)^2, P^2) = -[P^2(2m_b^2 + s'(2 - 3u) + P^2 v)]B_0(P^2 uv, m_b^2, m_b^2) + \left[\frac{1}{uv}((s'u + P^2 v)m_b^2 + s'^2 u(1 - 2u)\right.$$

$$\left. + s'P^2 v\right]B_0(s', 0, m_b^2) - \left[\frac{1}{uv}((s'u + P^2 v(1 - 2u))m_b^2 - P^4 v^2(1 + u) + s'^2 u(1 - 3u)\right.$$

$$\left. + P^2 vs'(1 + 3u^2))\right]B_0((1 - u)(s' - P^2 v), 0, m_b^2) + \frac{2}{uv}[(um_b^2 + vP^2 - u^2 s')$$

$$\times (vP^2(m_b^2 - us') + us'^2)]C_0(s', P^2 uv, (1 - u)(s' - P^2 v), 0, m_b^2, m_b^2).$$

B_0 and C_0 are the standard two-point and three-point functions, respectively:

$$B_0(p^2, m_0, m_1) = \frac{(2\pi\mu)^{4-D}}{i\pi^2} \int d^D q \{(q^2 - m_0^2 + i\epsilon)$$

$$\times ([q + p_1]^2 - m_1^2 + i\epsilon)\}^{-1},$$

$$C_0(p_1^2, (p_1 - p_2)^2, p_2^2, m_0, m_1, m_2)$$

$$= \frac{(2\pi\mu)^{4-D}}{i\pi^2} \int d^D q \{(q^2 - m_0^2 + i\epsilon)([q + p_1]^2 - m_1^2$$

$$+ i\epsilon)([q + p_2]^2 - m_2^2 + i\epsilon)\}^{-1}.$$

[1] R. Fleischer, Phys. Rep. **370**, 537 (2002).

[2] M. Beneke, G. Buchalla, M. Neubert, and C. T. Sachrajda,

Phys. Rev. Lett. **83**, 1914 (1999).

[3] M. Beneke, G. Buchalla, M. Neubert, and C. T. Sachrajda,

Nucl. Phys. **B606**, 245 (2001).

[4] J. Charles *et al.* (CKMfitter Group), Eur. Phys. J. C **41**, 1 (2005); W. N. Cottingham, I. B. Whittingham, and F. F. Wilson, Phys. Rev. D **71**, 077301 (2005).

[5] A. J. Buras, R. Fleischer, S. Recksiegel, and F. Schwab, Phys. Rev. Lett. **92**, 101804 (2004); Nucl. Phys. **B697**, 133 (2004); Acta Phys. Pol. B **36**, 2015 (2005).

[6] Y. Y. Keum and H. n. Li, Phys. Rev. D **63**, 074006 (2001); Y. Y. Keum, H. n. Li, and A. I. Sanda, Phys. Lett. B **504**, 6 (2001); Y. Y. Keum and A. I. Sanda, Phys. Rev. D **67**, 054009 (2003).

[7] M. Ciuchini, E. Franco, G. Martinelli, and L. Silvestrini, Nucl. Phys. **B501**, 271 (1997); M. Ciuchini, E. Franco, G. Martinelli, A. Masiero, M. Pierini, and L. Silvestrini, hep-ph/0407073; C. Isola, M. Ladisa, G. Nardulli, T. N. Pham, and P. Santorelli, Phys. Rev. D **65**, 094005 (2002); A. Deandrea, M. Ladisa, V. Laporta, G. Nardulli, and P. Santorelli, hep-ph/0508083.

[8] G. Buchalla and A. S. Safir, Phys. Rev. Lett. **93**, 021801 (2004); hep-ph/0406016.

[9] C. W. Bauer, D. Pirjol, I. Z. Rothstein, and I. W. Stewart, Phys. Rev. D **70**, 054015 (2004).

[10] T. Feldmann and T. Hurth, J. High Energy Phys. 11 (2004) 037.

[11] C. W. Chiang, M. Gronau, J. L. Rosner, and D. A. Suprun, Phys. Rev. D **70**, 034020 (2004).

[12] Y. Grossman, A. Hocker, Z. Ligeti, and D. Pirjol, hep-ph/0506228.

[13] A. Khodjamirian, Nucl. Phys. **B605**, 558 (2001).

[14] I. I. Balitsky, V. M. Braun, and A. V. Kolesnichenko, Nucl. Phys. **B312**, 509 (1989); V. M. Braun and I. E. Halperin, Z. Phys. C **44**, 157 (1989); V. L. Chernyak and I. R. Zhitnitsky, Nucl. Phys. **B345**, 137 (1990).

[15] M. A. Shifman, A. I. Vainshtein, and V. I. Zakharov, Nucl. Phys. **B147**, 385 (1979); **B147**, 448 (1979).

[16] V. M. Belyaev, A. Khodjamirian, and R. Ruckl, Z. Phys. C **60**, 349 (1993); V. M. Belyaev, V. M. Braun, A. Khodjamirian, and R. Ruckl, Phys. Rev. D **51**, 6177 (1995); A. Khodjamirian, R. Ruckl, S. Weinzierl, and O. I. Yakovlev, Phys. Lett. B **410**, 275 (1997); E. Bagan, P. Ball, and V. M. Braun, Phys. Lett. B **417**, 154 (1998); P. Ball and R. Zwicky, J. High Energy Phys. 10 (2001) 019.

[17] A. Khodjamirian, T. Mannel, and P. Urban, Phys. Rev. D **67**, 054027 (2003).

[18] A. Khodjamirian, T. Mannel, and B. Melić, Phys. Lett. B **571**, 75 (2003).

[19] V. M. Braun and I. E. Halperin, Phys. Lett. B **328**, 457 (1994); V. M. Braun, A. Khodjamirian, and M. Maul, Phys. Rev. D **61**, 073004 (2000).

[20] J. Bijnens and A. Khodjamirian, Eur. Phys. J. C **26**, 67 (2002).

[21] H. F. A. Group, hep-ex/0505100; see also http://www.slac.stanford.edu/xorg/hfag/.

[22] M. Gronau and D. London, Phys. Rev. Lett. **65**, 3381 (1990); M. Gronau, O. F. Hernandez, D. London, and J. L. Rosner, Phys. Rev. D **50**, 4529 (1994).

[23] J. Charles *et al.* (CKMfitter Group), Eur. Phys. J. C **41**, 1 (2005); see also http://ckmfitter.in2p3.fr.

[24] B. Aubert *et al.* (*BABAR* Collaboration), hep-ex/0507003.

[25] D. Bečirević and A. B. Kaidalov, Phys. Lett. B **478**, 417 (2000).

[26] A. J. Buras and L. Silvestrini, Nucl. Phys. **B569**, 3 (2000).

[27] A. Khodjamirian, T. Mannel, and N. Offen, Phys. Lett. B **620**, 52 (2005).

[28] F. De Fazio, T. Feldmann, and T. Hurth, hep-ph/0504088.

[29] M. Beneke and T. Feldmann, Nucl. Phys. **B592**, 3 (2001).

[30] A. G. Grozin and M. Neubert, Phys. Rev. D **55**, 272 (1997).

[31] I. I. Balitsky and V. M. Braun, Nucl. Phys. **B311**, 541 (1989).

[32] S. Eidelman *et al.* (Particle Data Group), Phys. Lett. B **592**, 1 (2004).

[33] P. Ball and R. Zwicky, Phys. Lett. B **625**, 225 (2005).

[34] A. P. Bakulev *et al.*, Phys. Rev. D **70**, 033014 (2004); **70**, 079906(E) (2004).

[35] A. Khodjamirian, R. Ruckl, S. Weinzierl, C. W. Winhart, and O. I. Yakovlev, Phys. Rev. D **62**, 114002 (2000).

[36] P. Ball and R. Zwicky, Phys. Rev. D **71**, 014015 (2005).

[37] D. J. Broadhurst and A. G. Grozin, Phys. Lett. B **274**, 421 (1992); M. Neubert, Phys. Rev. D **45**, 2451 (1992); E. Bagan, P. Ball, V. M. Braun, and H. G. Dosch, Phys. Lett. B **278**, 457 (1992).

[38] V. L. Chernyak and A. R. Zhitnitsky, Nucl. Phys. **B201**, 492 (1982); **B214**, 547(E) (1983).

[39] A. Khodjamirian, T. Mannel, and M. Melcher, Phys. Rev. D **68**, 114007 (2003).

[40] M. Beneke and D. Yang, hep-ph/0508250.